GeoScienceWorld
Lithosphere
Volume 2021, Article ID 7866617, 28 pages
https://doi.org/10.2113/2021/7866617

Lithosphere

Research Article

Late Quaternary Tectonics along the Peri-Adriatic Sector of the Apenninic Chain (Central-Southern Italy): Inspecting Active Shortening through Topographic Relief and Fluvial Network Analyses

Federica Ferrarini,[1,2] **J. Ramón Arrowsmith**,[3] **Francesco Brozzetti**,[1,2] **Rita de Nardis**,[1,2] **Daniele Cirillo**,[1,2] **Kelin X. Whipple**,[3] **and Giusy Lavecchia**[1,2]

[1]*DiSPUTer, Università degli Studi "G. d'Annunzio" Chieti-Pescara, Via dei Vestini 31, 66100 Chieti, Italy*
[2]*CRUST-Centro InteRUniversitario per l'Analisi SismoTettonica Tridimensionale, Via dei Vestini 31, 66100 Chieti, Italy*
[3]*SESE-Arizona State University, 781 E Terrace Road, Tempe, AZ, USA*

Correspondence should be addressed to Federica Ferrarini; f.ferrarini@unich.it

Received 30 April 2021; Accepted 12 August 2021; Published 10 November 2021

Academic Editor: Feng Cheng

Active compressional tectonics along the outer front of the Apenninic-Maghrebian chain (Italy) is well documented along the northern and central segments and in Sicily. On the other hand, the Southern Apenninic Outer Front (SAOF) orogenic activity is well established only until the Lower-Middle Pleistocene. We address the hypothesis of its subsequent late Quaternary activity in central-southern Italy (Abruzzo and Molise regions). We integrated topographic and fluvial network analyses along with morphotectonic investigation of fluvial terraces to identify evidence of differential rock uplift. We compared the results with the main geolithological units, known structural elements, and long-term deformation history from seismic line interpretation. We found variable evidence suggesting localized rock uplift in the Abruzzo region along the SAOF (Abruzzo Citeriore Basal Thrust segment) and inward structures on its hanging wall (Casoli-Bomba high), as well as along part of the Struttura Costiera thrust. Middle-to-Late Pleistocene deformation is constrained by terrace tilting and disruption along the Pescara river. Localized shortening along segments of the Apenninic Outer Front could explain the observed pattern of anomalies which is difficult to explain with long-wavelength regional uplift alone. Our reconstruction is consistent with the long-term deformation of the area and agrees with its seismotectonic setting. Despite the low deformation rate context and the peculiar geological setting which challenges the interpretation of the topographic and geomorphic signals, this study compels reconsideration, in terms of seismic hazard assessment, of the existence of late Quaternary active thrusting in central-southern Italy.

1. Introduction

Earthquakes are a major natural hazard in Italy. Most of the national territory is characterized by a long historical record of disruptive earthquakes [1]. The territory is in a zone of complex active tectonic deformation marked by contemporary extensional and contractional domains along the Apenninic chain [2]. The bulk of the seismic energy is released in the extensional domain [3]; however, moderately energetic sequences ($4.0 \leq Mw \leq 6.0$) with compressive/transpressive focal mechanisms have also occurred (in the last 50 years) along the outer sectors of the Apennines [4] (Figure 1) in areas characterized by shortening at rates ≃2 mm/y [5–8]. The unexpected shortening-related earthquakes that have occurred in northern Italy (e.g., Emilia Mw 6.1, 2012 seismic sequence in Figure 1) indicate the existence of seismogenic

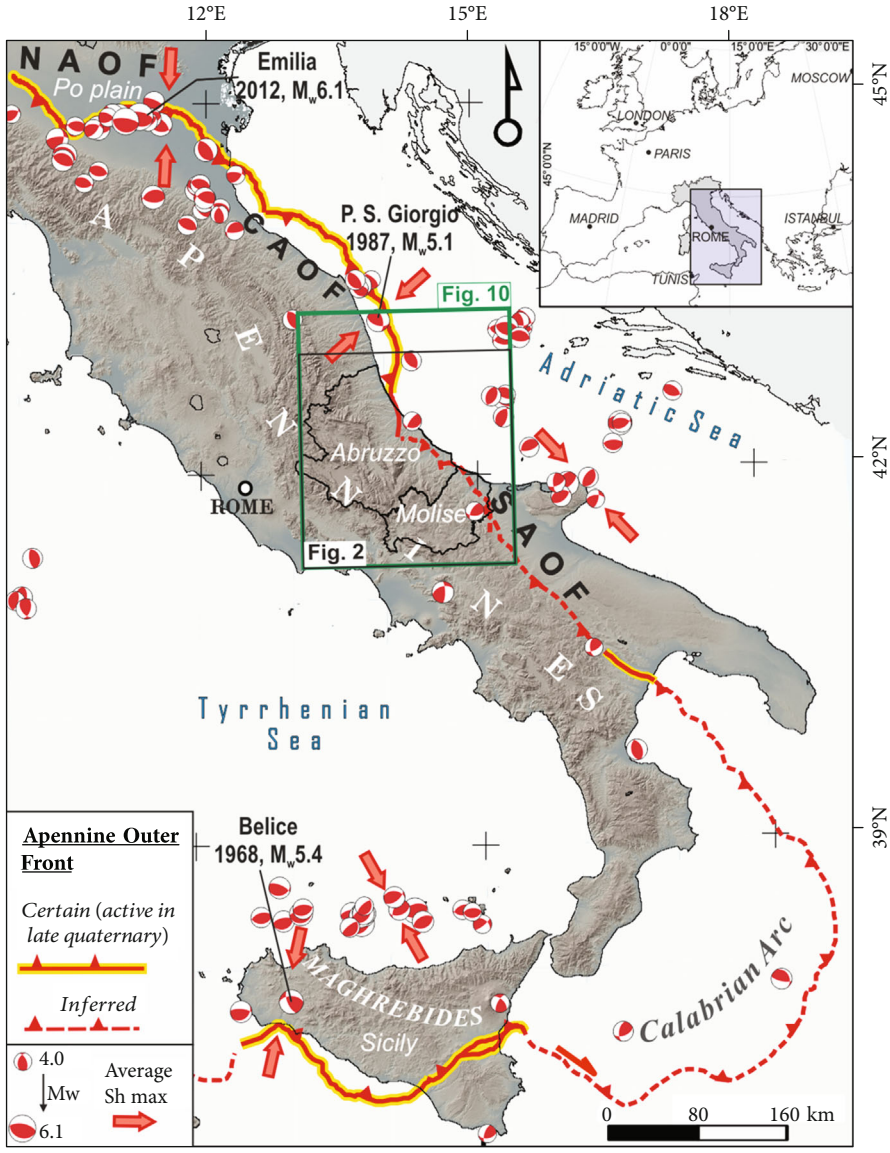

Figure 1: Present position of the Apenninic-Maghrebian outer front [16] with its arcuate traces and the compressive focal mechanisms available for the Italian peninsula and Sicily in the period 1905-2016 [4]. Key: NAOF: Northern Apenninic Outer Front; CAOF: Central Apenninic Outer Front. The red arrows represent (locally) the average direction of the maximum horizontal stress (Sh_{max}) as derived from the focal mechanisms along the different AOF segments. Location maps of Figures 2 and 10 are also reported (black and green rectangles, respectively).

sources along the outer sectors of the Apenninic chain [9–11]. Such structures require additional study and consideration for seismic hazard assessment in Italy.

The Apenninic-Maghrebian chain traverses NW-SE mainland Italy along a ~900 km long fold-and-thrust belt and connects with the E-W Maghrebian chain, in Sicily, through the Calabrian Arc (Figure 1). The belt reached its present setting following a progressive forelandward propagation of thrust sheets in response to several tectonic events during the Neogene [12–15]. The position of the Apenninic Outer Front (AOF) [16] can be outlined along three main arches corresponding (at a scale of hundreds of km) to the Northern Apenninic Outer Front (NAOF), the Central Apenninic Outer Front (CAOF), mostly located in the central Italy Adriatic offshore, and the Sicilian outer front along the Maghrebian domain in Sicily (Figure 1).

Evidence of ongoing shortening along the NAOF has been recognized in N-verging late Quaternary blind thrusts and folds inferred from geological and seismic data, in the western Po Plain and in the central and eastern Padanian plain [11, 17–19]. Triangular facets and tilting of alluvial terraces [20], quantitative analysis of topography [21], and tilting of geomorphic markers [22] have been used as evidence of NAOF late Quaternary (also Holocene) activity. The Emilia Mw 6.1, 2012 seismic sequence represents further seismogenic evidence of its activity (see Figure 1).

Along the CAOF, a prominent incision along the lower reaches of rivers flowing toward the Adriatic Sea has been

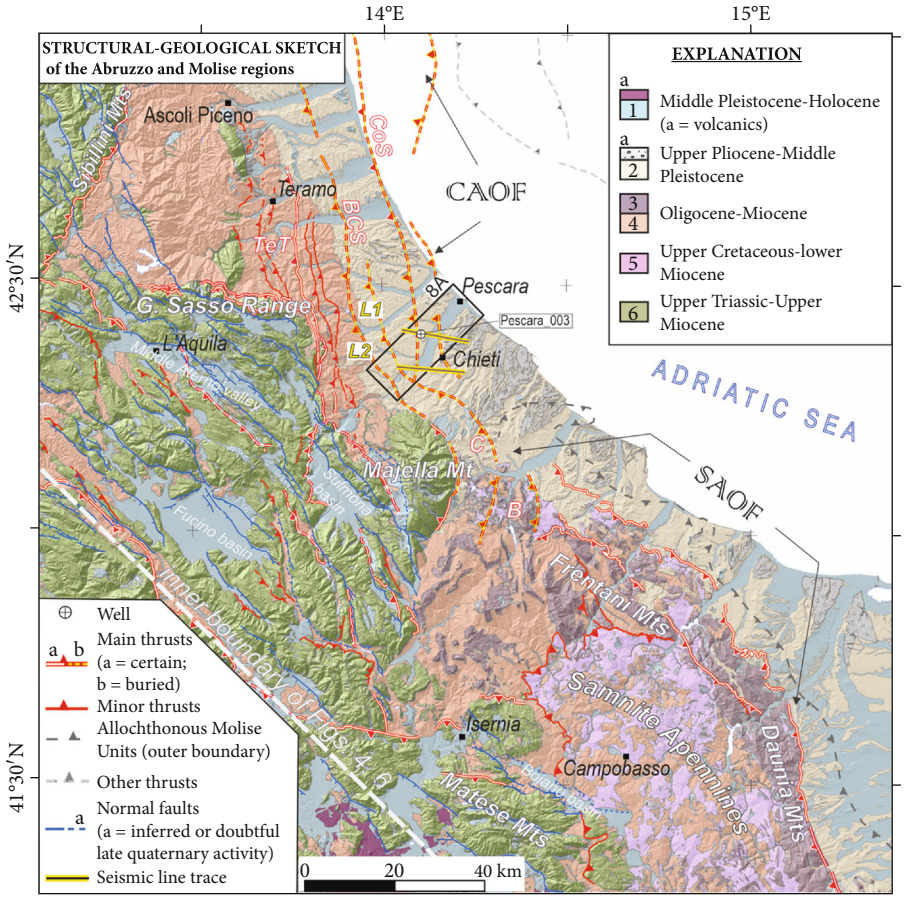

FIGURE 2: Structural-geological sketch of the Abruzzo and Molise regions (location map in Figure 1) with the principal geological units and structural lineaments. Geologic units derive from the Italian Geological Cartography at the 1 : 100,000 scale [86]. Key: (1) postorogenic (Middle Pleistocene-Holocene) continental deposits (coastal facies to fluvial deposits and fluviolacustrine, slope debris, and continental deposits) and volcanic rocks; (2) late orogenic deposits represented by late Pliocene-Middle Pleistocene marine successions (clays and sands) overlain by (a) Early-Middle Pleistocene conglomerates and sands; (3) Oligo-Miocene calcarenites, marls, and slaty marls; (4) Oligo-Miocene foredeep deposits (sandstones, marly sandstones); (5) Upper Cretaceous-lower Miocene inner-derived basinal units (argillites and varicolored scaly clays); and (6) Meso-Cenozoic (Upper Triassic-late Miocene) shelf carbonates (limestones and subordinately dolostones) and slope-to-basin and basinal deposits (limestones alternating calcareous marls, marls, cherty limestones, and cherts). Inset labeled 8A includes the area where the fluvial terrace analysis has been performed (Figure 8) and the well (Pescara_003) used for calibrating the major reflectors in the seismic line interpretation (L1 and L2 in Figure 9). The tectonic lineaments have been redrawn from numerous published papers and maps. Normal faults derive from [89–93]. Thrust/reverse faults derive from maps of the Italian Geological Cartography at the 1 : 100,000 scale [86], from maps of the Italian Geological Cartography at 1 : 50,000 [87, 88], and from [16, 85, 94–96]. TeT = Teramo thrust; BCS = Bellante-Cellino structure; CoS = Struttura Costiera; C = Casoli high; B = Bomba high.

explained by localized rock uplift associated with fold growth and active shortening [23]. The CAOF association with shallow-to-lower crustal instrumental seismicity (e.g., with the Porto S. Giorgio Mw 5.1, 1987 earthquake, Figure 1) has also been suggested (Adriatic Basal Thrust in [24–26]).

Along the Sicilian outer front, folds and incipient thrust fault formation and morphotectonic evidence of terrace uplift have been related to late Quaternary active shortening [27–36]. Its association with historical and instrumental earthquakes (e.g., Belice Mw 5.4, 1964 earthquake in Figure 1) has been also suggested [37, 38]. Ongoing shortening/transpressional deformation has also been inferred along the Calabrian Arc [39, 40] and in the Gulf of Taranto area [41].

On the other hand, orogenic activity along the NW-SE-trending Southern Apenninic Outer Front (SAOF in Figure 1) is well documented only until the Lower and part of the Middle Pleistocene [14, 42–45]. Only hints of younger activity have been reported along the Abruzzo piedmont of central Italy [46–48], and a possible association with historical earthquakes has been advanced [49–52].

In this paper, we inspect the late Quaternary shortening at the regional scale in the Abruzzo and Molise regions of Italy (Figures 1 and 2) along the SAOF and its northern (on land) connection with the CAOF. We test the hypothesis of its activity by considering that tectonic signals may be obscured by the geological setting. In fact, the SAOF and CAOF are buried under Plio-Pleistocene foredeep deposits [16, 43, 45, 53–57]. In addition, they belong to a sector characterized by very low deformation rates [6, 41, 58].

Topographic derivatives allow an assessment of the balance between tectonics (rock uplift) and erosion [59–67].

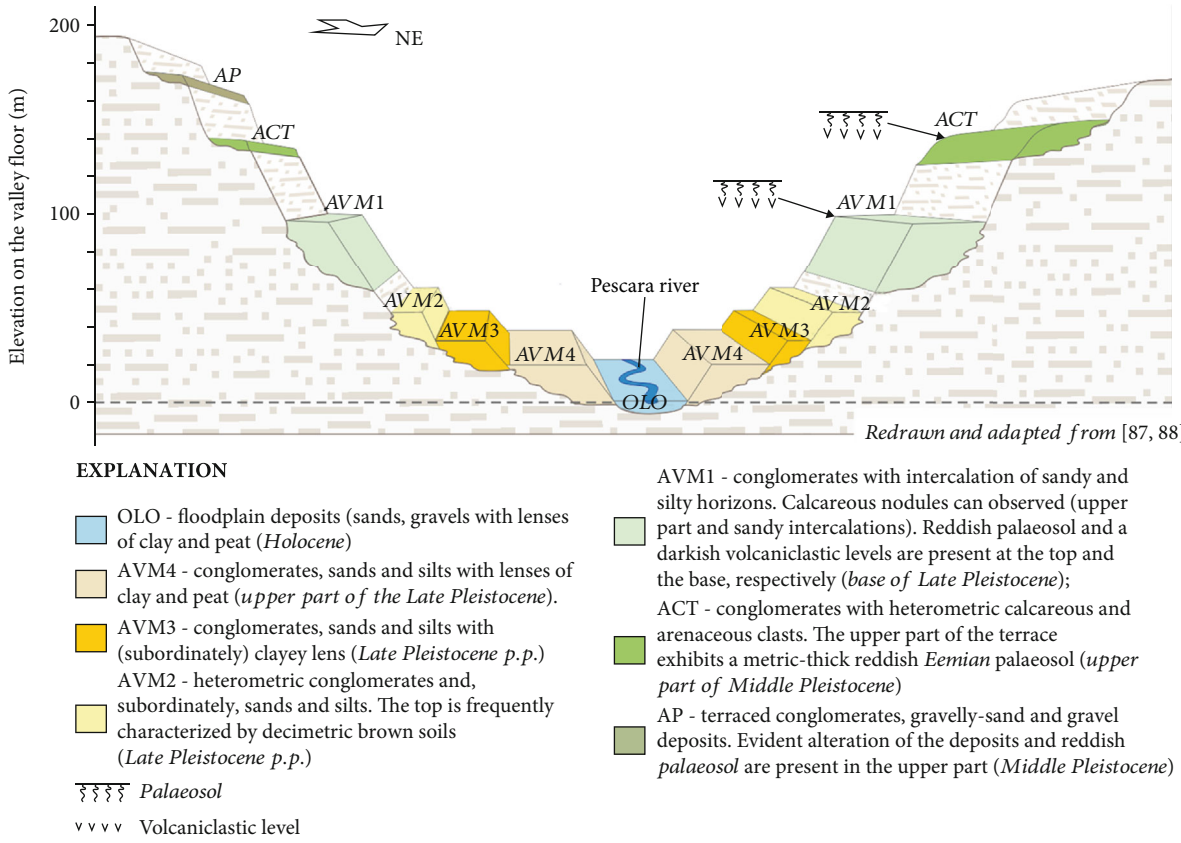

Figure 3: Morpho-lithostratigraphic sketch of the late Quaternary continental deposits along the Pescara river (redrawn and adapted from [87, 88]).

Topographic swath profiles, in particular, help to investigate large-scale features of topography [68, 69].

Fluvial network analysis is a common approach used to detect the transient response that rivers could exhibit as a consequence of changes in rock uplift rates (while attempting to account for differences in erodibility). Knickpoint detection and more advanced metrics are efficient tools for detecting signals of tectonic activity across erosional landscapes [62, 69–72], even in contexts characterized by low deformation rates [48, 73–75].

Lidar-derived digital terrain models (DTMs) enable remote identification of geomorphic features at the meter scale, providing valuable information for earthquake geology and tectonic geomorphology [76–79].

Seismic reflection profiles provide geometric descriptions of major shortening structures and of syntectonic sedimentary sequences [13, 80–84]. Their interpretations may relate the long-term deformation history of an area with evidence of active tectonics [18, 19].

By exploiting available high-resolution topography and the favorable orientation of the fluvial network with respect to the SAOF and CAOF (Figure 2), we integrated the above-mentioned methods and focused along the peri-Adriatic sector of the Apenninic chain (southern Abruzzo and Molise regions). We moved southeastward from the commonly accepted position of the CAOF [16, 85] which has been the locus of the 1987 P.S. Giorgio compressive seismic sequence (Figure 1). We computed local relief and residual maps, swath profiles, k_{sn} maps, and χ-z profiles to identify evidence of differential rock uplift and transient signals related to the activity of thrusts and/or reverse faults (black rectangle in Figure 1). We compared the results with the main rock units and structural elements and, as a case study in addition to and in comparison with the morphometric analysis, we investigated the morphotectonic setting of the middle-late Quaternary fluvial terraces preserved along the lower Pescara river valley and looked for the possible presence of displaced terraces (see inset 8A in Figures 2 and 3). In the same sector, we integrated the analysis with interpreted seismic reflection sections (Figure 2) to support a possible correlation between the shortening structures (eventually recognizable in the subsurface) and the pattern of relief and stream network anomalies detected in the topography and geomorphology. We summarize results and discuss them in light of the existent literature for the area, and we explore possible seismotectonic implications of the outcomes using a synthesis of published data.

2. Structural-Geological Background

In the Abruzzo and Molise regions, the outcropping rocks can be classified into six first-order geolithological units (Figure 2) which rely on [86]. In detail, they are as follows: (1) Quaternary (Middle Pleistocene-Holocene) postorogenic continental deposits represented by coastal facies to fluvial deposits (along the Adriatic sector) and fluviolacustrine,

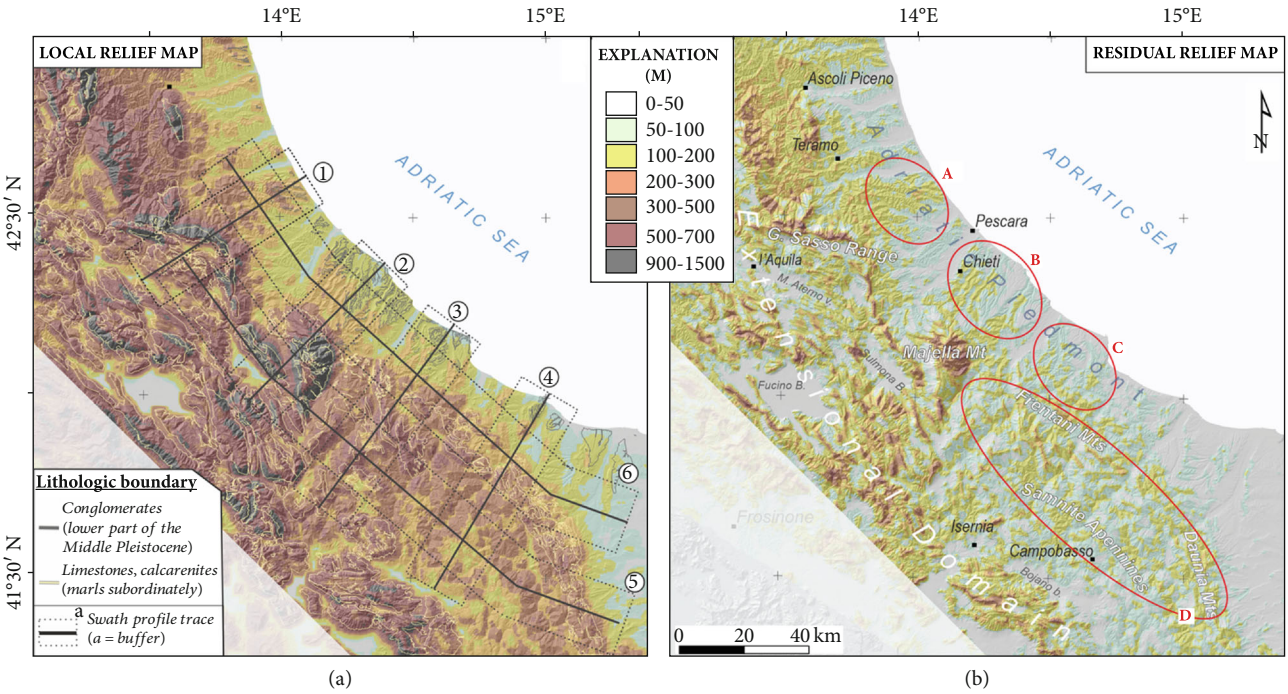

FIGURE 4: Topographic analysis for the study area showing (a) the mean local relief (over a 2.5 km rectangular neighborhood) and (b) residual relief. Panel (a) shows the traces of the swath profiles computed in this study (circled labels; see Figure 5). The names of the physiographic features in (a) are as in Figure 6(a). The red ellipses labelled A, B, C, D (in panel b) highlight areas where topographic anomalies, possibly related to local tectonic uplift, are noted and discussed in the text.

slope debris, and continental deposits (in the chain sector); (2) late orogenic deposits represented by late Pliocene-Early Pleistocene marine successions (clays and sands) overlain by (a) regressive, offshore prograding sequences of polygenic conglomerates carved into lagunal clays and silts (e.g., "*Ripa Teatina*" Fm *auctorum* in [87, 88]) (lower part of the Middle Pleistocene); (3) Oligo-Miocene calcarenites, marls, and slaty marls; (4) Oligo-Miocene foredeep and thrust-top basin deposits (sandstones, marly sandstones, and, subordinately, calcarenites and conglomerates); (5) Upper Cretaceous-early Miocene inner-derived basinal units (mostly argillites and varicolored scaly clays); and (6) Meso-Cenozoic (Upper Triassic-late Miocene) preorogenic sequences represented by shelf carbonates (limestones and subordinately dolostones) and slope-to-basin and basinal deposits (limestones alternating with calcareous marls, marls, cherty limestones, and cherts).

The different units were deposited on the southern Neotethyan passive margin, and starting from Late Tortonian-early Messinian, they were emplaced with a northeastern vergence onto the Adriatic foreland in response to the Neogene convergence between the European and African plates [15, 55]. The Apennines fold-and-thrust belt was formed with an overall in-sequence regional propagating model ([14, 45] and references therein, [97, 98]) and through local late Messinian-early Pliocene out-of-sequence reactivations, often accompanied by block rotations [99–101].

Evidence of contractional tectonics in this sector indicates activity during the Early Pleistocene (Gelasian-Calabrian transition: 1.8 Ma), in response to the last important phase of NE migration of the foredeep [14, 42, 45, 102]. More well-defined ages have been provided in the Marche-Abruzzi Apennines to post-Emilian (~1.2 Ma) and post-Sicilian (~0.7 Ma) tectonic phases [44, 103]. They have been tentatively correlated with unconformities and paleosols observed within the Lower-Middle Pleistocene marine and continental successions outcropping in the Molise region [104]. In general, the late Pliocene-Pleistocene contractional tectonic phases contributed to the first establishment of the Adriatic piedmont (Figure 4), a wide homocline gently sloping NE [105–108].

Starting from the late Miocene, along-axis extensional deformation affected the inner portion of the chain [98, 109, 110]. In the Abruzzo and Molise regions, this is well recognized along the Quaternary active (mainly) west-dipping normal faults with associated intracontinental basins [111–113]. This tectonics is confirmed by seismological [4], geodetic [6, 7], and structural-geological data [89–93, 114, 115].

2.1. Late Quaternary Evolution of the Abruzzo-Molise Peri-Adriatic Sector. The Middle-Late Pleistocene (post-0.7 Ma) tectonic evolution of the peri-Adriatic sector is usually inferred to be dominantly related to regional doming [44, 102, 116–121] and considered the result of a major geodynamic rearrangement responsible for the drastic braking, or ending, of the frontal thrust systems' activity. The origin of the doming is still debated (see among the others [98, 122–127]). The consequent uplift has been considered the main tectonic control on the late Quaternary landscape evolution of the existing piedmont. Deep fluvial downcutting and valley formation are widely observed along

the Abruzzo and Molise foothills and peri-Adriatic areas [107, 108, 128, 129]. Estimated uplift rates in the coastal sector of the Abruzzo region and the Gargano area range between 0.18 and 0.20 mm/y (Figure 7 in [44] and [116]). No significant deformation of Late Pleistocene sequences has been recognized based on the interpretation of seismic lines in the Adriatic offshore sequences [44].

2.1.1. The Pescara River Continental Deposits. For the terrace analysis that is presented in Section 3.4, we also provide a brief description of postorogenic continental deposits (study area in Figure 2, inset 8A).

Along the Pescara river valley, the late Quaternary continental deposits are represented by fluvial and alluvial fan environments and, secondarily, by coastal deposits and slope debris. From the older to the younger and from the highest to the lowest (Figure 3), they are referred to as synthems (names and descriptions as in [87, 88]) and are represented by Aielli-Pescina (AP), Catignano (ACT), and Valle Majelama (AVM). The latter has been further divided into four subsynthems. The deposits pertaining to the different synthems are arranged in staircase fill terraces, often associated with minor suites of strath terraces. For a more detailed description, we refer the reader to Supplementary Material S1 and the published geological maps [87, 88, 130].

The youngest deposits are represented by Holocene floodplain sands, gravels with lenses of clay and peat (along the valley floor of the main river and the lowest reaches of the main tributaries), littoral sands and gravels of coastal areas, and landslide and slope deposits (OLO).

3. Methods and Data

Relief and fluvial network analyses were performed over a wide area including both the southern Abruzzo and Molise regions (Figure 2). We focused along the peri-Adriatic sector, within a $\sim 70 \times 150$ km wide strip extending from the coastal to foothill areas and including the outer shortening structures reported in the literature and related to the SAOF and CAOF. Considering that extensional tectonics is not the topic of this study, we minimized our considerations of the inner Apenninic chain.

For both the topographic relief and fluvial network analyses, we used the 10 mpx resolution Digital Elevation Model raster dataset from Tarquini et al. (2007) (hereinafter DEM). For our computations, we combined GIS tools (ArcGIS Desktop by ESRI, v. 10.6.1) and MATLAB-based software: TopoToolbox [131, 132] and Topographic Analysis Kit (TAK) for TopoToolbox [133].

For the morphotectonic analysis along the Pescara river lower course, we used the maps at the 1 : 50,000 scale (CARG project [87, 88]). High-resolution topography (lidar data available from the Italian Ministry of the Environment; see 'Resources' in Additional Points) was used to extract the terrace tread heights in a swath along the river longitudinal profile.

Finally, seismic lines available from [134] were interpreted and in-depth converted using the MOVE Suite Software by Petroleum Experts Ltd. (see 'Resources' in Additional Points).

3.1. Relief Analysis: Topographic Relief Maps and Swath Profiles. To compute local and residual relief maps, we smoothed the DEM by using the Focal Statistics tool available in ArcMap and applying a moving mean over a 50 m window. We denote that raster surface R.

From R, we obtained the local relief using the Focal Statistics tool with the range statistic over a 2.5 km rectangular neighborhood. We choose this window assuming that it captures the most common ridge-valley spacing (along the coast). The resulting map is shown in Figure 4(a). According to the geolithological units (Figure 2), we reported over the relief map the boundary of the strongest rock types possibly having a role in the distribution of the anomalies (limestones/calcarenites and conglomerates).

To further highlight high relief features, we also computed the residual topography in the same area [63, 135, 136]. We obtained the bottom valley- and ridge-crest elevation values through the following steps: (1) extraction of two different fluvial network pixel sets, one from R (RS) and the other one (RS^-) from the inverted raster dataset (R^-); (2) conversion of RS and RS^- to ESRI polylines and then to point datasets (PRS and PRS^-); (3) extraction (from R) of the elevation values of PRS and PRS^-; and (4) raster creation *via* kriging interpolation (2500 m radius) from PRS^- and PRS to obtain *envelope* (E) and *subenvelope* (SE) surfaces, respectively. The residual topography is the vertical difference (i.e., E – SE). The map is shown in Figure 4(b).

We drew six swath profiles (20 km wide buffers), oriented both perpendicular (#1 and #2, 60 km length; #3 and #4, 70 km length) and parallel (#5, 180 km length; #6, 170 km length) to the SAOF-related shortening structures (traces on Figure 4(a)). The maximum, minimum, and mean elevations are projected onto the axis of the swath. For comparison, we also reported the (average) profiles of the local and residual anomalies using, in this case, a buffer of 10 km for the computation (Figure 5). The value has been chosen to capture the main features (but not approaching the average topography in the case of the local relief) and to avoid local effects.

3.2. Fluvial Network Analysis: Normalized Channel Steepness (k_{sn}). For a steady-state landscape, when the river incision rate is equal to the rock uplift rate, the power law function [137, 138]

$$S = k_s A^{-\theta}, \tag{1}$$

describes the change of the local channel slope (S) as a function of increasing the drainage area (A). The stream power parameters k_s and θ are the channel steepness index and channel concavity index, respectively [139].

The scaling relationship holds downstream of a critical threshold drainage area (A_{crit}) where a transition occurs from the divergent to convergent topographies or from the debris flow (colluvial channel) to fluvial processes [139–141]. A_{crit} typically falls in the range of 0.1-5 km^2 ([62] and references therein). The slope-area relation (1) also applies upstream of the transition between the bedrock and alluvial channels where detachment-limited conditions typically prevail [139, 142, 143].

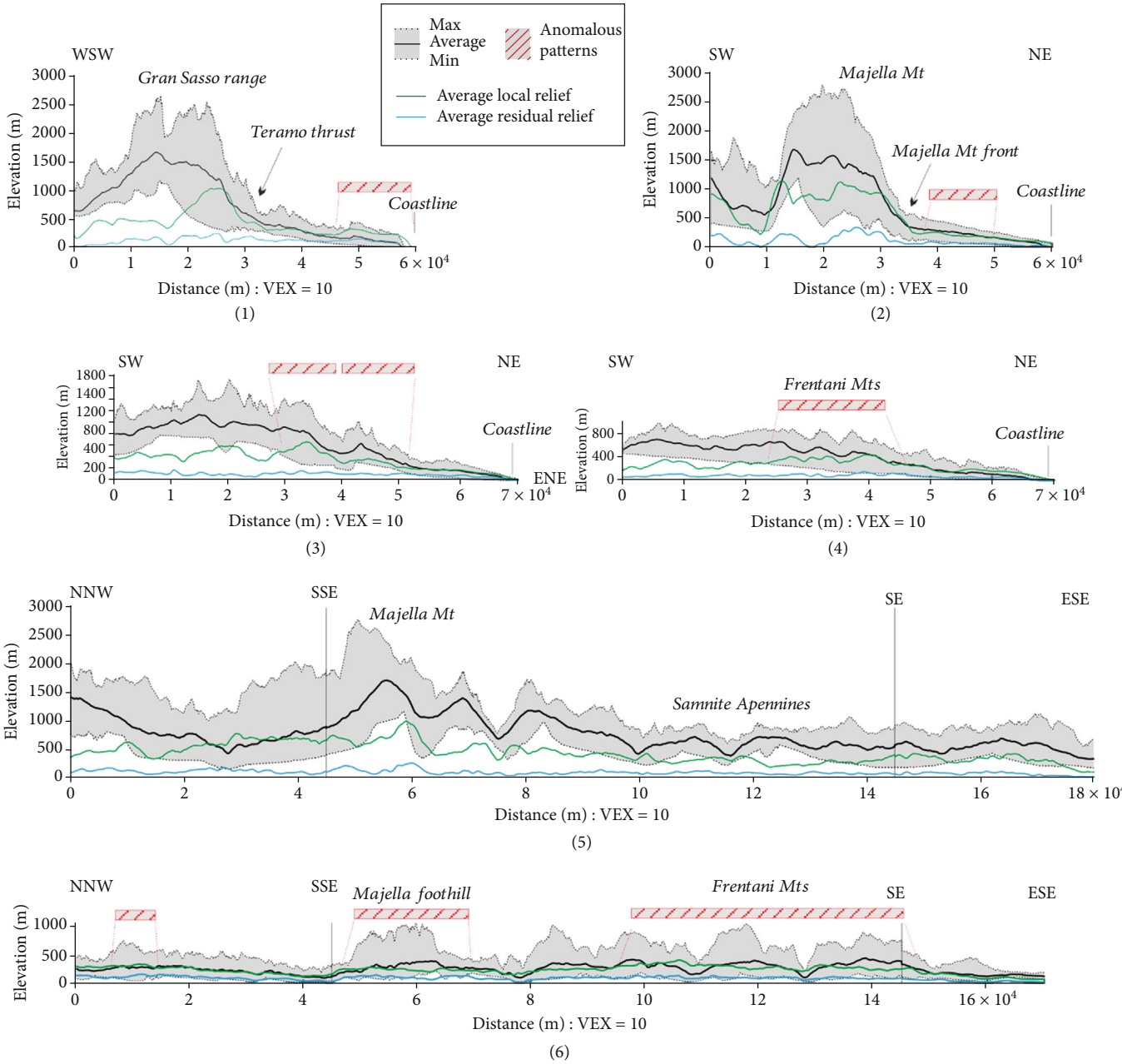

FIGURE 5: Topographic swath profiles (20 km width) across the SAOF of Abruzzo and Molise regions and inner belt (location in Figure 4). Curves represent the maximum, minimum, and mean elevation profiles projected onto the axis of the swath. The green and blue lines are the average local and residual relief, respectively. Dashed bars represent sections along the swaths which suggest differential uplift (potential shortening-related anomalies), as deduced from the relief analysis. See detail in the text.

After DEM filling, we first extracted the fluvial network in the study area (Figure 2) *via* the TopoToolbox (TT) basic functions [131, 132]. We considered, for the along-river analysis described later, a subset of streams with trunk length ≥ 15 km (Figure 6(a)) and preliminarily divided them into two sets based on the length and drainage basin area (Figure 6(b)). For ease of understanding, we refer to each river by its number (from 1 to 15 in Figure 6(a)).

We considered the $A_{crit} = 0.1\,km^2$. Even if this value represents the lower threshold of the critical drainage area [70, 140], it was chosen to foster better k_s regression considering that the rivers showed a slope-area scaling relationship typical of fluvial channels also along their upper course (Figure 6(b), 1; Supplementary Material S2). In this way, we also attempted to identify subtle signals that may have more chance to persist along lower-order river tributaries.

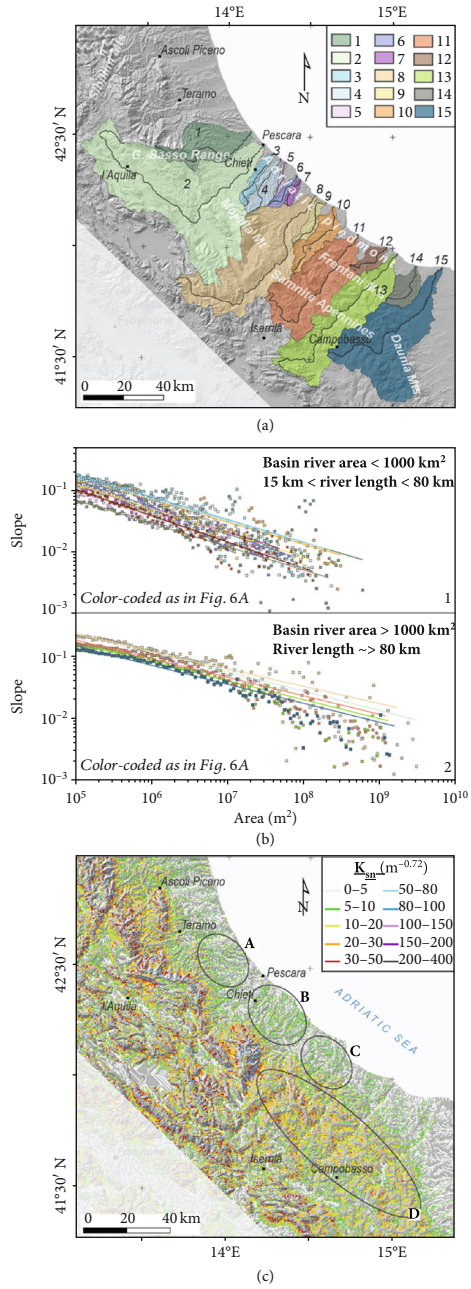

Figure 6: Fluvial network analysis along the SAOF and CAOF of the Abruzzo and Molise regions. (a) Color-coded drainage basins analyzed in the study (1: Saline; 2: Aterno-Pescara; 3: Alento; 4: Foro; 5: Arielli; 6: Moro; 7: Feltrino; 8: Aventino-Sangro; 9: Osento; 10: Sinello; 11: Trigno; 12: Sinarca; 13: Biferno; 14: Saccione; and 15: Fortore). (b) log S-log A plots of the smaller (1) and bigger (2) rivers (color-coded as in (a)); related values of θ and k_s are reported in Table 1. (c) Map of the spatial distribution of k_{sn}. The black ellipses labeled A–D highlight areas where k_{sn} anomalies, possibly related to shortening-driven uplift, have been observed and discussed in the text.

To overcome k_s-θ dependency [143], we used the stream power law for a reference concavity [62, 70, 136]:

$$S = k_{sn} A^{-\theta_{ref}}. \quad (2)$$

Commonly, $\theta_{ref} = 0.45$ is used, as steady-state channels should fall into a relatively restricted range of concavities ($0.4 \le \theta \le 0.6$). Slope-area regressions indicate that most of the rivers in our study area have concavity values lower than 0.4 (Figure 6(b) and Table 1; Supplementary Material S2). We thus consider a $\theta_{ref} = 0.36$; this value represents the average of all computed concavities.

We are aware that the regression to compute the concavity index is affected by the chosen A_{crit}. Nevertheless, in Supplementary Material S3, a sensitivity test demonstrates that the low value we have considered ($A_{crit} = 0.1\,km^2$) has not affected the analyses following in this work (i.e., χ -transformed river profiles and knickpoint detection; see Section 4.2.1).

By using $\theta_{ref} = 0.36$ and A_{crit} and exploiting the "KsnChiBatch" TAK function (hereinafter TAKf; [133]), we first computed a k_{sn} map (Figure 6(c)). Free access to data obtained with this approach is provided in the COLOSSEO-1 [Data set] (see in Data Availability).

3.3. Along-River χ-z Plots and k_{sn} (Knickpoint) Analyses. Given its capacity to highlight tectonic forcing in conditioning the topography of river basins [72] and to enhance possible along-stream disequilibrium conditions, we exploited the integral approach [144]. Integrating both sides of the stream power law with respect to the distance yields

$$z(x) = z(b) + A_0^{-\theta} k_s \chi. \quad (3)$$

χ is an integral function of position along the channel, with dimensions of length, and is also expressed as

$$\chi = \int_{x_b}^{x_0} \left(\frac{A_0}{A(x)} \right)^{\theta} dx, \quad (4)$$

where the integration is performed upstream from the base level (x_b) to the location x along a channel. The integral form of the slope-area relation predicts that at the steady state, for the uniform runoff, rock strength, and sediment caliber, χ river profiles will be identified by a straight line when the typical θ value of the river has been identified.

To identify transient signals along the river profiles, we investigate them by using χ-z plots. The method allows us to identify the knickpoint-bounded caliber with deflections from the predicted linear behavior [144]. It has main advantages in reducing the scatter due to noisy topographic data by avoiding the calculation of the slope along the channels. Using a reference concavity also allows for comparison among rivers with different drainage areas.

We produced for each of the channel trunks (#1 to #15 in Figure 6(a)) a χ-z plot by using the "*KsnProfiler*" TAKf, and $\theta_{ref} = 0.36$ has been incorporated into Equation (3). We identified along-river χ-value knickpoints, and we isolated river segments corresponding to an abrupt change in the k_{sn} which has been computed through linear regression. For each picked segment, the corresponding (average) k_{sn} is reported in Table 2.

Table 1: Main features (length and drainage basin area) of the rivers analyzed in this study together with the river concavity index (θ) and the channel steepness index (k_s) computed for each of them from log S-log A regression (see Figure 6(b)). In the table are also reported the approximate along-river distance (from the outlet) at which the transition between the bedrock and alluvial channel conditions ($X_{b\text{-}a}$) is inferred to occur and the reference (Ref) the information comes from (this Table is also available in the COLOSSEO-1 [Data set], see in Data Availability).

#	Name	Trunk length (km)	Watershed area (km^2)	k_s	θ (theta)	Average θ (theta)	$X_{b\text{-}a}$ (km)	Ref
1	Saline	78.24	614.62	12.73	0.37		29	[85, 123]
2	Aterno-Pescara	166.71	3174.52	8.97	0.31		37	[85–87]
3	Alento	37.00	118.25	12.65	0.37		9	[85–87]
4	Foro	40.90	235.46	9.57	0.35		24	[85, 87]
5	Arielli	22.30	41.87	10.35	0.41		—	—
6	Moro	25.93	72.65	4.88	0.44		4	[48, 85]
7	Feltrino	17.15	50.99	10.29	0.39		—	—
8	Aventino-Sangro	133.19	1755.85	5.80	0.28		23	[96, 123, 181]
9	Osento	36.78	124.39	12.14	0.40		17.5	[96, 151, 182]
10	Sinello	53.42	311.27	10.37	0.36		25	[148, 180]
11	Trigno	99.19	1221.91	5.80	0.28		11	[96, 123, 183]
12	Sinarca	29.45	137.32	14.82	0.43		2	[96, 123]
13	Biferno	115.09	1308.18	5.71	0.31		22.5	[96, 104, 123]
14	Saccione	34.33	217.04	5.54	0.38		17	[96, 123]
15	Fortore	109.46	1596.74	5.54	0.38	0.36	44	[123]

To distinguish rock-type dependency from rock uplift [145], we plotted the rock-type transitions over which each river flows, according to the geological map in Figure 2.

In addition, to consider possible effects of the transition from the bedrock to alluvial channel conditions, we also attempted to detect its approximate location (hereinafter $X_{b\text{-}a}$). To this aim, we integrated information coming from both the available geological cartography and the specific papers, looking for multiple indications of alluvial conditions (e.g., continuous outcrops of fluvial terrace deposits and widening of alluvial plains, decreasing in the slope of the river profiles, and evident river meandering). We reported the $X_{b\text{-}a}$ location (from the outlet) along each of the χ-z plots (Figure 7(a)), and summarized in Table 1.

The comparison allowed us to distinguish between knickpoints: (1) falling in the contractional domain, possibly driven by active rock uplift (upstream increase of k_{sn}, black stars); (2) related to rock-type variation, or bounding segments connected to an upstream decrease of k_{sn}, or more likely due to extensional tectonics (in the inner sector of the study area) (white stars); and (3) with doubtful interpretation (yellow stars) located close to rock-type changes, or dams or other anthropogenic modifications of the channel profiles, or falling where alluvial conditions are supposed to occur (between the outlet and the $X_{b\text{-}a}$ or in the proximity of the latter).

The results of the χ-z plot analysis are shown in Figure 7(a). The complete output for each river, including (trunk) longitudinal profiles, χ-z plots, and k_{sn} averaging, as well as the residual between the actual river profiles and the theoretical ones (according to $\theta_{ref} = 0.36$), is presented in Supplementary Material S6.

3.4. Fluvial Terrace Analysis along the Pescara River. In order to detect signals of active shortening and derive differential uplift affecting late Quaternary deposits, we examined the lower course of the Pescara river. There, anomalous geometry in the terrace treads (defined by the late Quaternary synthems described above and illustrated in Figure 3) could be reasonably related to active deformation younger than the Middle Pleistocene. We focused on the north side of the valley where the different fluvial terrace orders are well preserved (see Section 2.1.1, Figure 3; Supplementary Material S1). To ease the detection of even subtle topographic signals, we exploited the resolution (1 to 2 m resolution, vertical and horizontal accuracy ~ ±5 cm) of lidar data available for the sector (see Section 3). We built a DTM raster and projected onto it the mapping of the different late Quaternary terraces (Figure 8). The distinction within the Late Pleistocene terraces (Figure 3; Supporting Material S1) fostered our attempt to highlight late Quaternary deformation.

We drew the Pescara along-river longitudinal profile and projected onto it the same terrace tread heights along the first 42 km upstream from the mouth (black rectangle in Figures 2 and 8(a)) focusing on the north side of the valley, where the terraces are better preserved. We used a swath methodology approach along a path mimicking the Pescara river's bends and the general setting of the terraces (dashed line in Figure 8(a)). We used a buffer (semiwidth on the north side of the path) of 2.5 km. Locally, we choose to perform smaller swath sections with a smaller buffer (e.g., in the area of the Nora and Pescara river intersection, Figure 8(a)) to avoid including the elevation of terraces located along the tributaries. Results are shown in Figure 8(b).

3.5. Seismic Line Interpretation in the Abruzzo Peri-Adriatic Area. We interpreted two seismic sections which cross the leading edge of the outer thrust faults in the study area (Figure 2). These sections (Figures 9(a) and 9(c)), labelled

TABLE 2: k_{sn} values computed by linear regression and for the different segments picked along the transformed river profiles (χ-z plots) analyzed in this study (see also Supplementary Material S6). For each river, the first k_{sn} value reported is represented by the first value regressed along the picked segment from the mouth to the first knickpoint (i.e., field "mouth to k_{sn} 1"). To follow, upstream, the values reported represent the k_{sn} value between two adjacent knickpoints (e.g., "k_{sn} 1-2" stands for k_{sn} between the 1st and 2nd picked knickpoints). Bold values correspond to k_{sn} increases interpreted as tectonic-related. Asterisks refer to knickpoints with doubtful interpretation (this Table is also available in the COLOSSEO-1 [Data set], see in Data Availability).

#	NAME	MOUTH TO k_{sn} 1	k_{sn} 1-2	k_{sn} 2-3	k_{sn} 3-4	k_{sn} 4-5	k_{sn} 5-6	k_{sn} 6-7	k_{sn} 7-8	k_{sn} 8-9	k_{sn} 9-10	k_{sn} 10-11	k_{sn} 11-12	k_{sn} 12-13	k_{sn} 13-14
1	Saline	**4.95***	9.16	71.47	44.41	182.78	21.76	5.65	15.18	26.32	—	—	—	—	—
2	Aterno-Pescara	**4.34***	15.28	3.79	65.45	9.13	5.27	3.19	15.24	6.16	19.45	15.39	—	—	—
3	Alento	**3.32**	8.65	27.36	**11.28***	26.57	13.53	—	—	—	—	—	—	—	—
4	Foro	**5.72***	9.92	12.65	**22.60***	44.37	—	—	—	—	—	—	—	—	—
5	Arielli	5.50	**3.71**	6.88	**5.72**	12.29	4.51	—	—	—	—	—	—	—	—
6	Moro	5.24	**0.79***	**4.05**	**9.53**	23.42	7.35	—	—	—	—	—	—	—	—
7	Feltrino	5.96	**4.72**	7.18	**4.12**	7.51	—	—	—	—	—	—	—	—	—
8	Aventino-Sangro	9.02	**16.76***	49.83	15.77	7.36	54.34	3.68	13.91	7.43	34.29	8.29	1.66	28.12	6.07
9	Osento	**4.17***	**7.32**	20.85	16.07	1.57	—	—	—	—	—	—	—	—	—
10	Sinello	6.56	**10.11**	23.30	17.01	54.38	10.10	—	—	—	—	—	—	—	—
11	Trigno	9.06	21.71	34.95	7.12	18.54	4.79	2.01	10.10	—	—	—	—	—	—
12	Sinarca	3.48	6.57	6.61	—	—	—	—	—	—	—	—	—	—	—
13	Biferno	6.69	10.14	7.39	5.07	31.68	21.61	10.38	—	—	—	—	—	—	—
14	Saccione	1.46	**3.87**	5.59	7.41	—	—	—	—	—	—	—	—	—	—
15	Fortore	2.29	**8.09**	19.82	6.08	—	—	—	—	—	—	—	—	—	—

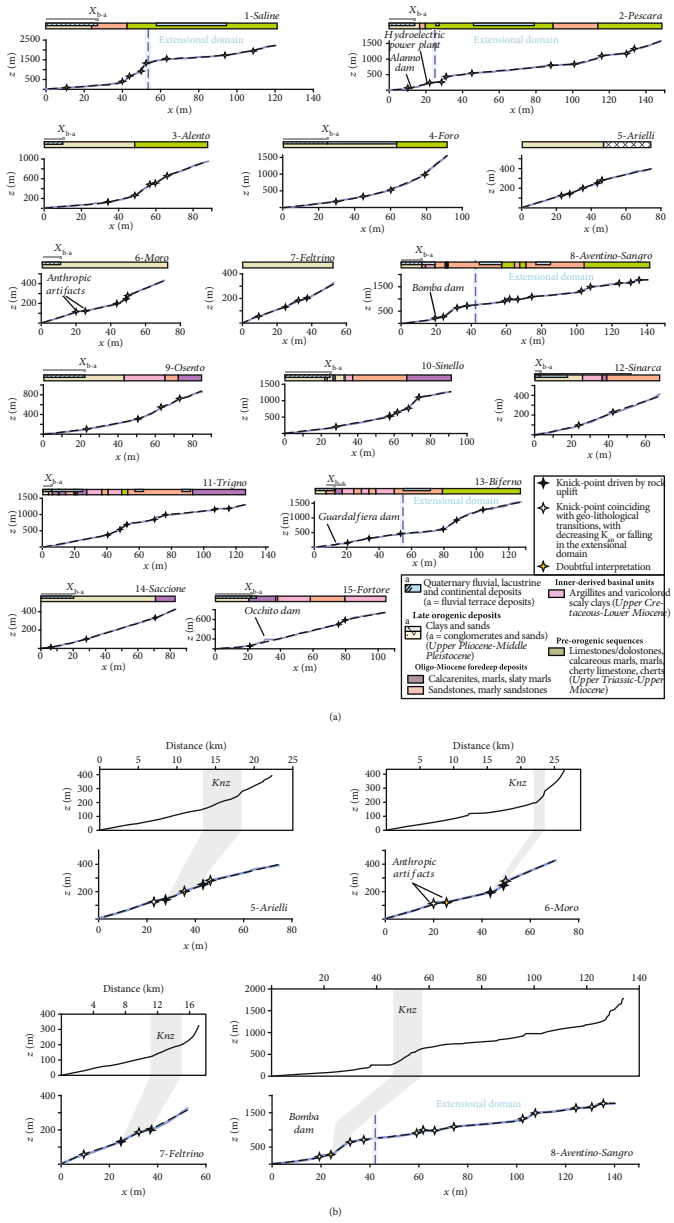

FIGURE 7: χ-z plot analysis along the rivers analyzed in this study and close-up views on some of them through comparison between the transformed and nontransformed (longitudinal) river profiles. (a) χ-z plot analysis along the rivers of the subset of streams analyzed in this study (see text for details). For clarity, the river's name is associated with the drainage basin number as in Figure 6. The dashed black lines show the linear regressions used to determine the normalized channel steepness index (k_{sn}) between two adjacent knickpoints. Stars correspond to the knickpoint-bounded segments showing changes in k_{sn} (see also Table 2). Black stars bound the segments connected to an upstream increase of k_{sn} falling in the shortening domain and potentially driven by active tectonics (i.e., not related to lithologic transitions). White stars mostly bound the segments connected to an upstream decrease of k_{sn} (possibly deriving from lithological transitions). They can also indicate the k_{sn} increase in the extensional domain or minor lithologic changes in the limestones (inner sector of the study area). In both the latter cases, these knickpoints are not taken into consideration in our analysis and data interpretation. Yellow stars mark knickpoints with doubtful interpretation (see text for details). $X_{b\text{-}a}$ indicates the approximate location (along the χ-z plots) of the transition from the bedrock to alluvial channel conditions (see text for details). Colored bars above each profile represent the rock units over which the river flows. Colors correspond to the map rock types shown in Figure 2. Among the other Quaternary deposits, only extensive lacustrine (rivers #14 and #15), alluvial fan (river #4), and intramountain basin deposits (rivers #1, #2, #8, and #13) have been reported with the bars. The dashed (vertical) light blue line represents the outer limit of the extensional tectonics; knickpoints have been indicated but not interpreted beyond this limit. (b) Comparison between the transformed and nontransformed (longitudinal) river profiles with examples of deviations from the theoretical profile. Key for the longitudinal profiles: Knz = knickzone. Key for the transformed profiles as in (a).

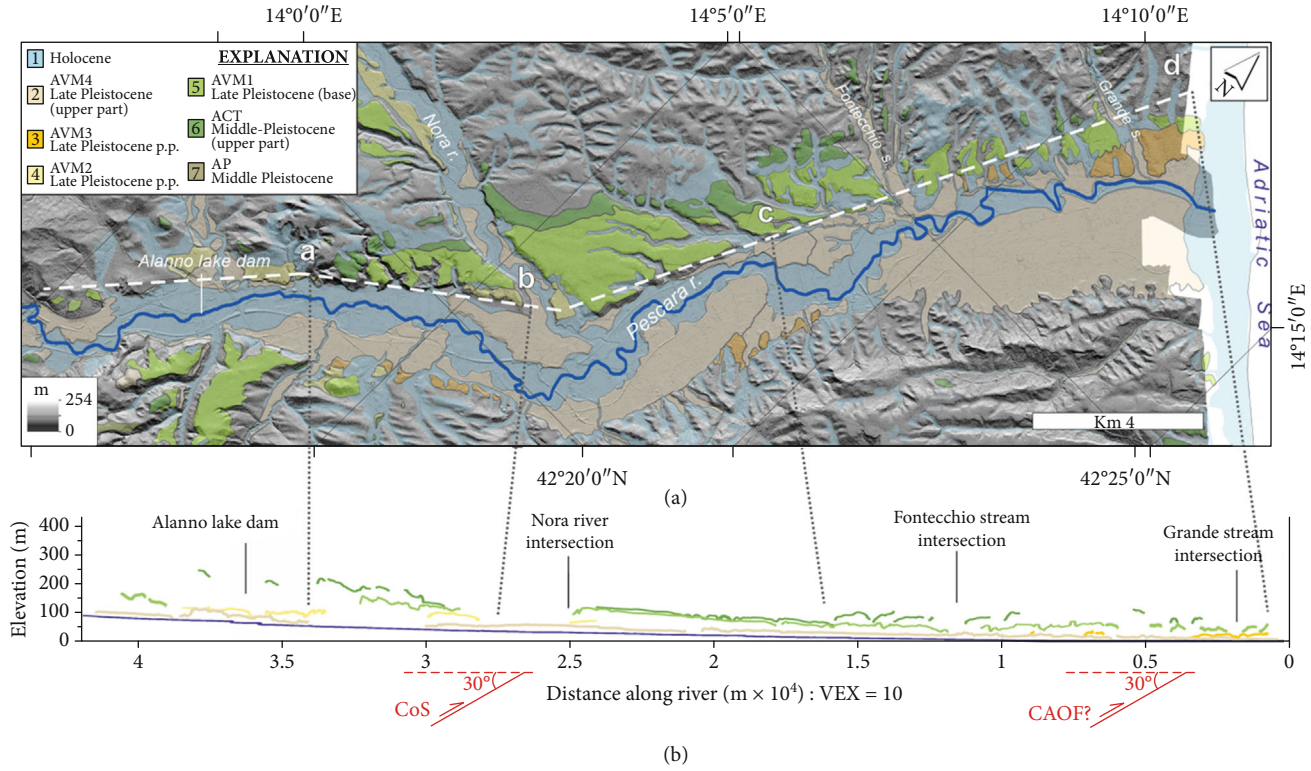

FIGURE 8: Fluvial terrace analysis along the Pescara river (see also in Figure 3). (a) Hillshade from lidar imagery (1 m-pixel resolution) overlain by late Quaternary terraces (scale 1 : 50,000) mapped in the area as reported from the CARG project [87, 88]. Acronyms: ACT: Catignano; AVM: Valle Majelama. Key: 1: Holocene deposits; 2: AVM4 (upper part of the Late Pleistocene); 3: AVM3 (Late Pleistocene p.p.); 4: AVM2 (Late Pleistocene p.p.); 5: AVM1 (base of Late Pleistocene); 6: ACT (Middle Pleistocene p.p.); 7: AP (Aielli-Pescina). (b) 42 km along-river longitudinal profile of the Pescara river with the projection of the terrace treads (only the left side; see text for details). The white dashed line in (a) is the swath profile trace (buffer 2.5 km) used to compute the mean elevation of the terrace outcrop (see text for details). The profile is vertically exaggerated (VEX = 10x). Key: CoS = Struttura Costiera; CAOF = Central Apenninic Outer Front.

in [134] as PEF-08-87 (https://www.videpi.com/deposito/videpi/allegati/2976.pdf) and PES-07 (https://www.videpi.com/deposito/videpi/sismicatitoli/all%203_Linea_PES-7.pdf), are hereinafter referred to as L1 and L2, respectively (for the original, available version of the seismic lines, see also Supplementary Material S4 and S5, respectively). They have been initially interpreted in paper copies and then gathered into the MOVE Suite PetEx software package (see 'Resources' in Additional Points). The quality of the seismic lines is not uniform because they were acquired with various sources of excitation (mainly vibroseis and rarely explosives). However, they provide usable images of the subsurface down to pseudo-depths of about 3.5–4.0 sec (two-way time, hereinafter twt) corresponding to depths of 6-8 km [81, 83, 146].

3.5.1. Seismic Stratigraphy. The quality of the seismic reflection signal is much better on the L1 profile than on the L2 profile (Figure 9). Consequently, the definition of the main seismostratigraphic facies and the corresponding units is mainly based on the analysis of L1 whereas the correlation between the two sections is made possible thanks to the recognition of some major reflections and the stratigraphy of the Pescara_003 well (https://www.videpi.com/deposito/pozzi/profili/pdf/pescara_003.pdf), the latter positioned very close to the profile traces (see location in Figure 2).

From bottom to top, the seismic facies are (Figure 9(a), rectangular inset) as follows: (i) Upper Triassic-late Miocene carbonate multilayer, (ii) Early Pliocene turbidites, and (iii) late Pliocene-Pleistocene shallow-water coastal, deltaic, and nearshore deposits. The correspondence between the seismostratigraphic units and the regional stratigraphy can be confidently established through the comparison with the stratigraphy of several boreholes of eastern Abruzzo, including the aforementioned calibration wells [83, 134].

The Meso-Cenozoic carbonates generally show low-amplitude heterogeneous reflections, except for some well-defined continuous and parallel ones located in the upper part, probably corresponding to Cretaceous marly horizons of the Marne a Fucoidi Fm [97, 147]. In the lower portions of the sections, the Triassic evaporites (usually characterized by light and transparent facies) cannot be easily recognized because of the poor quality of the signals at pseudo-depths > 4 sec twt. Conversely, the top of the carbonate multilayer is everywhere recognizable due to the strong impedance contrast characterizing the interface between the calcareous and pelitic rocks.

The Early Pliocene sedimentary prism is characterized by a nearly transparent lower interval, related to a stack of lithified beds of massive sandstones, followed upward by

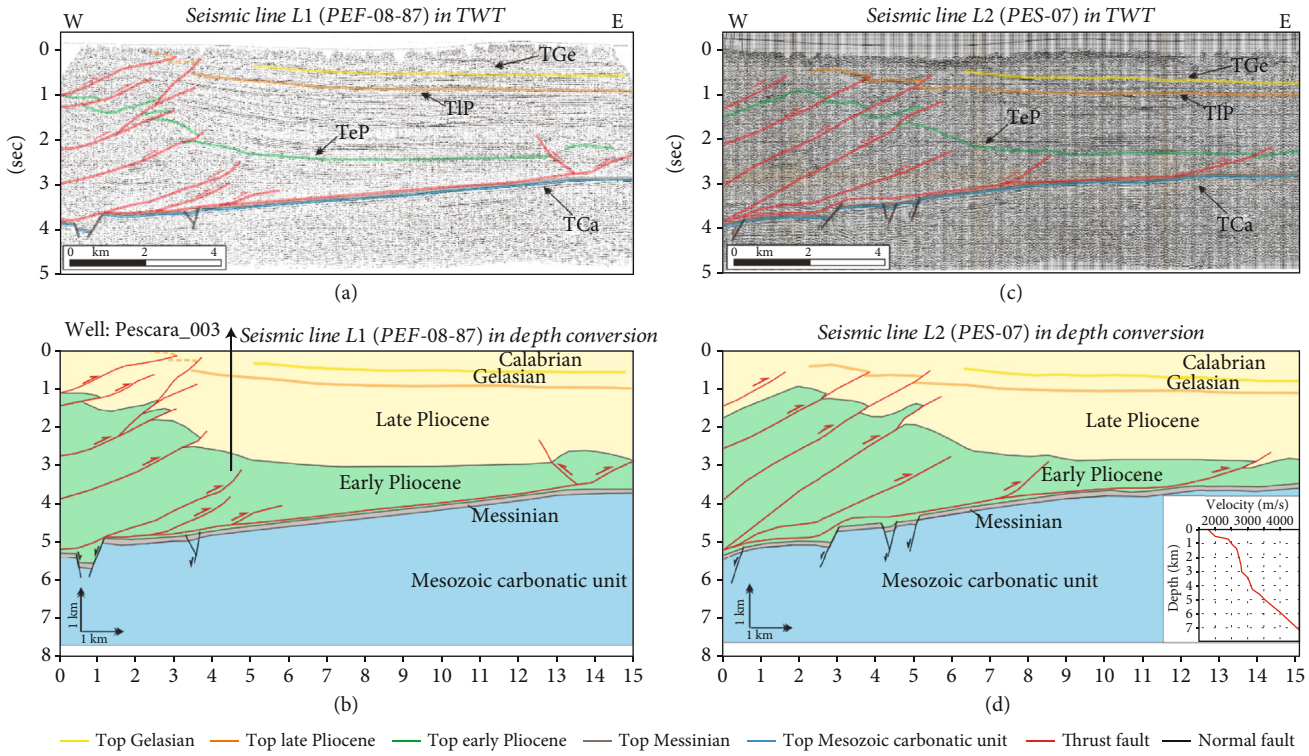

FIGURE 9: Seismic sections L1 and L2 interpreted in this study (PEF-08-87 and PES-07, respectively, from [134]). The L1 and L2 seismic sections (traces in the map of Figure 2) are shown in panels (a) and (c), respectively. Key: TCa = Top Carbonates; TeP = Top early Pliocene; TlP = Top late Pliocene; TGe = Top Gelasian (see text for details). The depth conversions of the key reflectors are shown in panels (c) and (d). The velocity model used for the conversion is reported in the lower right inset of panel (d). The location of the Pescara_003 well used for calibrating the major reflectors is also reported in the map of Figure 2.

subparallel, medium-amplitude, and laterally continuous reflectors, referable to thick-bedded basinal turbidites.

Finally, the late Pliocene-Pleistocene succession consists of a stack of well-packaged subparallel reflections (offshore pelites containing tabular sand bodies) alternating with intervals in which scattered low-continuity reflectors (thick massive clay deposits) occur. In the upper part of the Pleistocene deposits, the quality of the signal is poor and nearly transparent facies prevails, showing minor low-angle reflections, oblique with respect to the average bedding trend.

The boundaries among these major seismostratigraphic facies correspond to four key reflectors (Figures 9(a) and 9(c)): (1) TCa (Top Carbonates): the interface between the Meso-Cenozoic multilayer (locally corresponding to the Messinian evaporites) and the overlaying foredeep deposits; (2) TeP (Top Early Pliocene): the unconformable transition between the early Pliocene turbidites and the base of the late Pliocene-Pleistocene succession (within the latter, a further weak but rather continuous reflection, lying 1-1.6 sec twt above the TeP, marks an appreciable change of seismic facies); (3) TlP (Top late Pliocene); and (4) TGe (Top Gelasian): biostratigraphic data from the calibration wells which suggest that it approximates the Gelasian-Calabrian boundary (1.8 Ma).

4. Results

4.1. Topographic Analysis. The relief maps and swath profiles computed across the CAOF and SAOF in the southern Abruzzo and Molise regions indicate topographic anomalies delimited by the main tectonic and physiographic features of the study area.

In the local relief map (Figure 4(a)), the highest anomalies (up to 1500 m) can be observed in the Teramo area, along the G. Sasso range, on the frontal slope of the Majella Mt and in the Frentani Mt area. Along the Samnite Apennines, a modest signal in the local relief is evident (up to 700 m). In the sector running from the Adriatic coast inward, within a distance of 10-20 km, moderate local relief values (up to 900 m) are present. The trend decreases toward the coast and toward the southeast. In general, the relief correlates with the topography inherited from older shortening phases (see Figure 2) and, more recently, with the active extensional tectonics (close to the intracontinental basins, e.g., the Sulmona basin).

When comparing the local relief anomalies with the main geolithological units (Figure 2), the rock type influences the relief distributions. The highest relief is systematically located where the Meso-Cenozoic limestones, or the Oligo-Miocene calcarenites and marls, crop out (Figures 2 and 4(a)). Analogously, the decreasing relief along the coastal sector is related to the gentle NE dip of the Early-to-Middle Pleistocene conglomerates overlying the marine succession and cropping out along the Adriatic piedmont.

Residual relief anomalies (Figure 4(b)) persist south of Teramo and all along the coast (100-300 m) (inset A), as well

as in the foothill region adjacent to the Majella Mt (100-200 m) (inset B), from the Frentani Mts to the coast (100-300 m) (inset C), and across the Molisean hillslope (Frentani and Daunia Mts and Samnite Apennines: 100-500 m) where the signal is more scattered (inset D).

The particularly high anomaly persisting along the southern slope of the Majella Mt (900-1500 m) coincides with an additional lithological variation [85] between the Upper Jurassic-Upper Cretaceous carbonatic platform limestones and the Upper Cretaceous (Cenomanian-Maastrichtian) marly transitional-to-basin *facies*. We did not report the distinction of the different *facies* in the carbonatic units because the entire realm—except for Majella Mt—belongs in proximity or within the extensional domain which was out of our target. Nevertheless, we take it into account and attribute the evident (local) residual anomaly to a lithologic control.

The comparison of the previous results with the general pattern of the landscape is more evident along with the swath profiles (SW) of Figure 5:

(i) SW1 shows in the first 15 km a high average elevation (~1500 m) related to the inherited (contractional) topography of the Gran Sasso range as well as a peak in the local relief and an increase in the residual relief close to and up to the Teramo thrust (TeT in Figure 2), respectively; these are reasonably connected with the late Quaternary activity of the west-dipping normal faults of the area (Figure 2). Starting from ~30 km along the swath, a sudden topographic drop-off can be observed east of the TeT. Northeastward, a clear anticorrelation between the maximum and minimum elevations is evident. In the last 15 km of the profile, the elevation increases together with both the local and residual relief anomalies (dashed bar in Figure 5)

(ii) SW2 shows an average topography of 1500 m across the Majella massif and a drop on both sides. Similar to SW1, the clear anticorrelation on the west side of the profile is reasonably related to the activity of the Sulmona basin's normal fault (see Figure 2), but also eastward both local relief (often higher than 1000 m) and residual relief (up to 400 m) remain high. Eastward of the Majella thrust, the average topography decreases abruptly, as well as the residual and local relief

(iii) SW3 shows that the average topography stands between 800 and 1000 m along the first 25 km of the profile. A first increase in the local relief, not followed by the residual, can be observed at about 20 km from the beginning of the profile. A more relevant bimodal peak is instead between 30 and 50 km from (dashed red bars in Figure 5) where the average elevation starts to decrease. In the same segment, a slight increase of the residual relief, standing on a quite constant elevation of ~160 m, can also be pointed out

(iv) SW4 shows that the average elevation stands around 800 m for the first 28 km of the swath. Starting from this point, it decreases linearly toward the sea level while the local relief shows an increase between 25 and 45 km (dashed red bars in Figure 5). The residual relief is scattered, in the southeastern sector of the study area (see Figure 4(b)), and also along this profile stabilizes at about 150 m before decreasing close to the coast

(v) SW5 shows that the average topography and the anticorrelation between the maximum and minimum profiles are strongly conditioned by the extensional tectonics along the first ~60 km of the profile SE-ward of the Majella massif. The average elevation decreases linearly to 500-600 m and shows evident dissection by the fluvial network (mostly perpendicular to the swath), particularly evident between 60 and 80 km. Nevertheless, all the profiles are correlated and the residual relief is nearly constant

(vi) SW6 shows that the average elevation along the Adriatic piedmont is constant and remains below ~300 m until the profile intercepts the northeastern slope of the Majella Mt. Along this section, an anomaly affecting both the local and residual profiles can be noticed between 10 and 15 km. Starting from ~45 km, the topography is affected by the foothill physiography of the Majella and Frentani Mts. Here, the minimum and maximum elevations are everywhere anticorrelated, thus forcing the average elevation everywhere to 350-400 m and suggesting noticeable carving of the fluvial system. Local and relief profiles are correlated with the former increasing and standing around 600-700 m throughout the Frentani Mt area

4.2. Fluvial Network Analysis

4.2.1. Spatial Distribution of the Normalized Channel Steepness and χ Indices. When considering the sector crossed by the external shortening structures related to the CAOF and SAOF (see Figure 2), two different domains can be distinguished from the channel steepness analysis (Figure 6(c); we discard in our consideration the inner extensional domain— see Figure 2). A ~20 km wide strip, belonging to the southern Abruzzo-Molise piedmont and the Adriatic coast, has widespread low k_{sn} values. However, the areas (A–C in Figure 6(c)) have higher k_{sn} ranging between 5 and 20 m (-0.72). The values increase considerably in all the sectors on the hanging wall of the SAOF and (on land) CAOF, on the southern slope of Majella Mt and across the Frentani Mts (D in Figure 6(c)). The highest values can be observed in the inner sector of the Apenninic belt (extensional domain).

The k_{sn} regions are in good agreement with zones of both the high local and residual relief (Figures 4(a) and

4(b)). However, the general consideration that the higher and lower clusters correlate with the high and less competent geological units, respectively (Figures 2 and 4), must be taken into account. The relief anomaly distribution implies that the k_{sn} map alone is not enough to distinguish unequivocally uplift related to thrust activity from the lithological control.

On the other hand, the along-river χ-z analysis (Figure 7(a) and Table 2) turned out more successful in highlighting clues of localized uplift. In fact, bedrock conditions persist along most of the rivers' course or for all of it (#5, #7), making the interpretation of the knickpoints reliable, especially in the foothill areas. Nevertheless, for some of the rivers with lengths higher than ~100 km (rivers #1 and #2), the onset of alluvial river conditions locate in correspondence with the Adriatic piedmont (Figure 7(a) and Table 1), thus making doubtful the interpretation.

In some cases (rivers #5, #6, and #7 in Figures 7(a) and 7(b)), the knickpoints possibly driven by active rock uplift are not isolated deviations from the theoretical concave-up river profiles but are likewise spatially gathered in knickzones [148] (Knz, in Figure 7(b)), the latter also evident along the relative nontransformed (longitudinal) profiles. This feature is particularly obvious along river #8 (Figure 7(b)) where the Knz is prominent. We marked the knickpoint characterizing it as doubtful (yellow star in Figures 7(a) and 10) due to the proximity (~1 km) to a lithologic transition. Nonetheless, the k_{sn} increase is relevant (see also Table 2); we thus cannot exclude also an uplift component contributing to the χ-z along-river values.

On the whole, the spatial distribution of the knickpoints—marking increases in the k_{sn} over the picked segments—pointed out clustering of those likely driven by active tectonics (black stars in Figures 7(a) and 10). Most of them locate within the late Pliocene-Early Pleistocene marine successions of the Adriatic piedmont and Majella foothill (rivers #1 to #7 and #9). To the southeast, the knickpoints are also located within the Oligo-Miocene foredeep deposits (rivers #8 and #10) and within the Upper Cretaceous-early Miocene argillites and scaly clays (#9). From rivers #11 up to #15, no evidence of differential uplift can be inferred, with the exception of the Saccione (#14). All other knickpoints coincide with rock-type transitions, or with decreasing k_{sn}, or falling in the extensional domain. Even when the increases in k_{sn} appear to correspond to the SAOF contractional structures (rivers #12 and #15), they cannot be ascribed unequivocally to a tectonic origin (Figures 7 and 10 and Table 2).

4.3. Evidence of late Quaternary Deformation from Fluvial Terrace Analysis. The morphotectonic analysis of the late Quaternary terraces preserved along the northern bank of the lower Pescara river provides additional information in a sector where the topographic metric analysis does not indicate uplift (Figures 4(a), and 4(b)).

The combined use of lidar topography data and Quaternary geology shows a general downstream convergence of the projected terrace treads with local deviations (Figure 8(b)). The oldest terraces (ACT and AVM1) slope gently and consistently toward the coast. Analogously, the younger AVM2 treads show the same geometry, even if with a less prominent dip. Interestingly, ACT and AVM1 exhibit an evident disruption west of the Nora river intersection (from A to B in Figures 8(a) and 8(b)).

We interpret the observed tilting of the terraces as evidence of post-Middle Pleistocene deformation unlikely relatable to regional and large-scale uplift. Using terrace treads for tectonic purposes must be done with caution. Nevertheless, the AVM terrace deposits which crop out along the Pescara river valley are exclusively attributed to the fluvial environment and not to (mixed) fluvial-alluvial or coastal-delta facies (e.g., the older ACT synthem or "*Ripa Teatina*" Fms, respectively) (see Section 2). We can reasonably exclude the terrace modifications (and dip increasing) as a consequence of post-depositional (local-scale) contributions (e.g., colluvium, alluvial fans); thus, the warping may be explained as the result of deformation after deposition.

The AVM1 terrace tread, in particular, provides the basis to estimate uplift rates given the (fluvial) genesis and the relatively well-constrained age (base of Late Pleistocene) and its lateral continuity.

We suggest a possible correlation of the terrace deformation with the buried compressional structures reported in the Pescara sector, in particular with the Struttura Costiera thrust [149] (CoS in Figures 2 and 10).

Following [150] and the number of RSL (sea-level rise) curves compared in the study, the high-stand period also recorded in the Mediterranean at ~125 ky before present (marine isotopic stage MIS5e) raised the sea level to approximately the current one. The period corresponds to the age of AVM1 that, during its deposition, had approximately the same reference level. From MIS5e, a continuous low-stand period (with some oscillations) followed and drove the deposition (and carving) of the younger fill terrace orders. After MIS2 (~20 ky before the present), the sea level rose again until approaching the present one. No further sea-level transgressions have been documented in more recent times.

The evidence that the AVM1 terrace tread stands around a maximum elevation of ~150 m (see between A and B in Figure 8(b)) and was tilted (that cannot be depositional) suggests that starting from the Late Pleistocene, the uplift rate in the sector exceeded the sea-level ingression rate, given the possibility to observe, at present, younger terrace deposits also close to the coast.

We thus estimate an approximate surface uplift value of ~0.8 mm/y, averaged over 125 ky. In the case of a localized (vs. regional) uplift consequent to a fault activity, this value would account for a slip rate of ~1.6 mm/y along a theoretical 30°-dipping buried thrust, if considering the vertical component of the slip. In this scenario, the correlation of the terrace deformation with the activity of the buried CoS reported in the Pescara sector (Figures 2 and 10) could be advanced.

Finally, we are less confident about the tectonic meaning of the disruption affecting all the terrace orders between the Fontecchio and Grande streams (from C to D in Figures 8(a) and 8(b)). Nevertheless, the deformation pointed out along

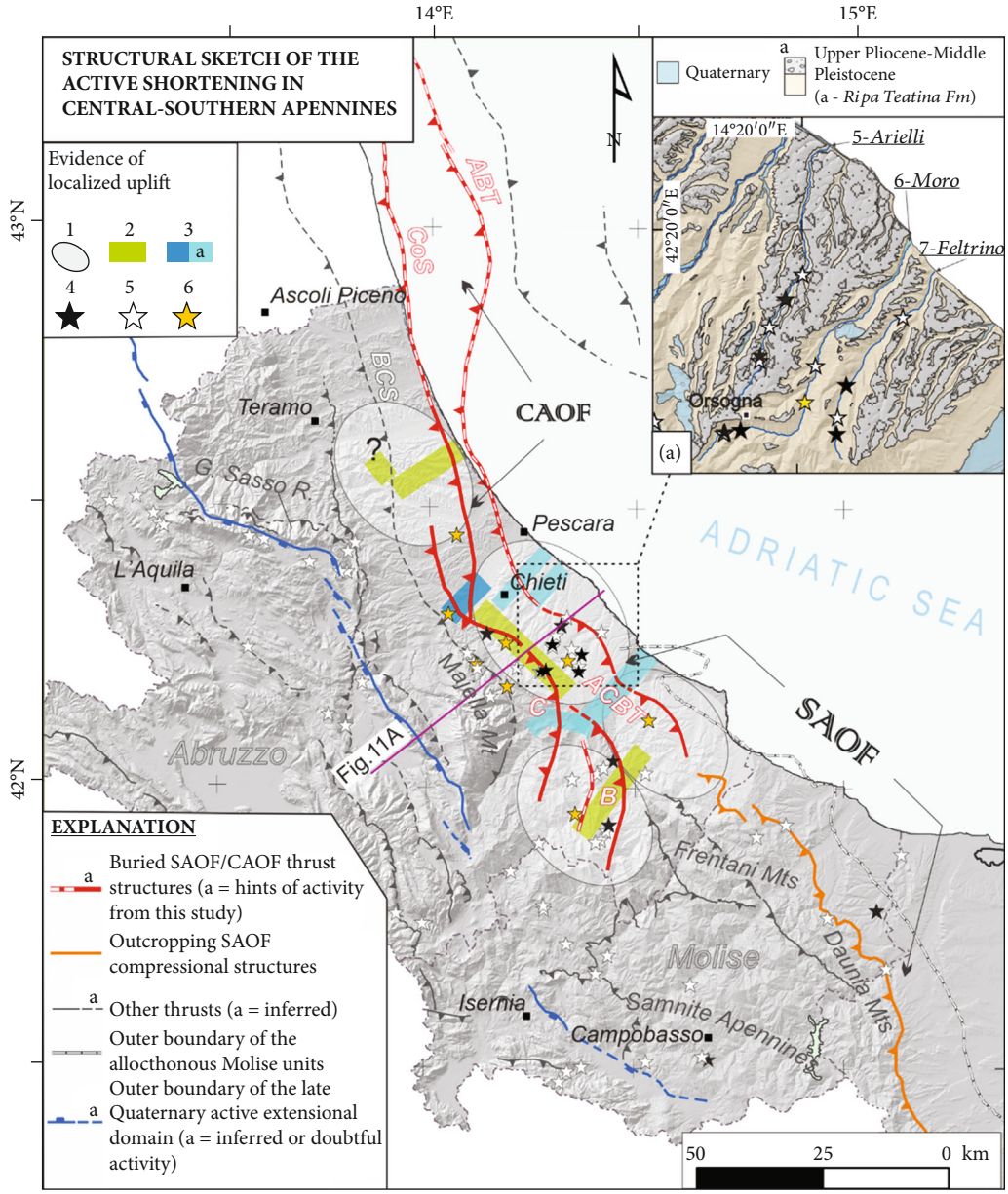

FIGURE 10: Structural sketch of the active NE-SW shortening in the central-southern Apennines (location map in Figure 1) with evidence from the different approaches discussed in this paper and comparison of results with additional (compiled) data on the seismotectonic setting of the area. Key: 1: anomalous areas contemporarily highlighted by local, residual, and k_{sn} maps; 2: topographic anomalies from swath profiles; 3: anomaly from the late Quaternary fluvial terrace tread pattern and disruption (a = from [48]); 4: tectonic-related knickpoints from along-river χ-z plots. For completeness, also non-tectonic knickpoints (5) and those with doubtful interpretation (6) have been reported. Names of the thrust structures as in Figure 2. Inset (a): detail of the relationship between rock units and knickpoints (from along-river χ-z plots) along the Abruzzo Adriatic piedmont. River numbers as in Figure 6. The geolithological units are color-coded as in Figure 2. Note the tectonic-related knickpoints located in the bedrock units (late Pliocene-Early Pleistocene clays and sands) along the Moro and Feltrino rivers.

the same terrace orders (named T2 and T3 in [48]), a few kilometers SE and along the Alento (#3) and Foro (#4) rivers (see the light blue strips in Figure 10), supports similar post-Middle Pleistocene deformation (or younger) along the outer CAOF (Adriatic Basal Thrust (ABT) in [24]) and related structures (Figures 2 and 10).

4.4. Subsurface Evidence of late Quaternary Deformation along the SAOF. The lines L1 and L2 continue for ~15 km in the W-E direction through the Pescara valley (map trace in Figure 2) crossing nearly orthogonally, in their western parts, the N-S-trending anticlines at the CAOF hanging wall. Our interpretation of the L1 and L2 seismic lines is driven by the recognition of the three key reflectors TCa, TeP, and TGe described above. Their presence with good continuity, all over the sections (Figures 9(a) and 9(c)), led us to highlight the main tectonic features and to make the following observations:

(i) TCa is evident on both the L1 and L2 sections as a prominent high-amplitude reflection, not affected by thrusting; it suggests the geometry of a gently dipping regional monocline which deepens westward from ~3 to 5 s twt and is affected by minor extensional faults possibly originating during the late Miocene foreland flexure that preceded the setting of the foredeep

(ii) TeP reflection is subhorizontal in the central-eastern part of the sections (at a depth of ~2.3 sec twt) while rising remarkably in the western sector where it is displaced and folded by the west-dipping splays of the CAOF; in its outer sector, the basal thrust localizes along the TCa causing the decollement of the early Pliocene turbidites from the Mesozoic carbonates

(iii) The progressive angular unconformity observed at the base of the Pliocene succession and its westward thickening suggests that (a) the onset of the foredeep stage occurred between the Late Messinian and the basal Pliocene, that (b) significant subsidence occurred during the early Pliocene in the absence of contractional deformations, and that (c) the beginning of CAOF activity, in the studied sector, postdates the TeP

The interpretation of the L1 and L2 profiles was converted to depth and turned into the geological sections (Figures 9(b) and 9(d)) by attributing to the seismostratigraphic units the interval Vp values obtained from the Pescara_003 well data (see graph in Figure 9(d), lower right inset). The depth conversion provides the thicknesses in meters of the stratigraphic units and the correct trajectories of the thrust faults.

Within the evident imbricate fan, the uppermost splays (coinciding with the CoS; see Figure 2) show the most recent activity; in fact, they displace the whole Pliocene unit and bend—and probably offset—also the Pleistocene succession. Close to the western border of both the sections, the poor quality of the shallowest seismic signals does not allow us to ascertain whether the westernmost thrust faults have reached and displaced the topography, but this does not exclude it. The lower and more external thrust (coinciding with the CAOF leading edge, Figure 2) only displaces the TeP.

5. Discussion

5.1. Overview. The working hypothesis of this study is that the SAOF, and its northern connection with the CAOF, could have been active in the late Quaternary, similar to other seismogenic segments of the AOF (NAOF, Sicilian Outer Thrust). Our multidisciplinary approach integrating topographic and fluvial network analyses, morphotectonic investigation of fluvial terraces, and seismic reflection interpretation locally supports this hypothesis.

The local relief map (Figure 4(a)) first addressed the investigation in sectors showing different elevation ranges and high localized topography.

The comparison between the local and relief profiles with the swaths (Figure 5) defined "strips" where anticorrelation of the maximum and minimum topography coincides with an increase in the local and residual relief. The comparison suggests areas of differential uplift which locate in the Adriatic piedmont (SW1, north of Pescara), in the foothill sector east of the Majella Mt (SW6) and southeast of the massif (SW3), close to the boundary between the Abruzzo and Molise regions (light green strips in Figure 10). This evidence agrees with the interpretation of the k_{sn} values' distribution (Figures 6(c) and 10). From both the analyses, however, a possible lithological influence on the anomalies cannot be excluded. The anticorrelation between the maximum and minimum elevations observed in the Frentani Mt area (SW4 and SW6 in Figure 5) does not support, alone, evidence of localized uplift.

We recognize that the topographic analysis alone does not discriminate lithological influences (Figure 2). As a matter of fact, landscape evolution has been demonstrated to exhibit dependency from lithology or structural setting (e.g., bedding attitude) which, in turn, modulates the rock erodibility [151, 152]. Rock resistance, on the other hand, can be nonuniform across the landscape because the main erosional agents (rivers, landslides, etc.) operate at different spatial and temporal scales ([153] and references therein). Topography's lithologic dependency has been partially confirmed in our study by the observed correlation between the higher values in the local and residual relief (in absolute terms) with the hardest rock types cropping out in the investigated area (e.g., limestones and calcarenites, Figure 4). No peculiar dependency has been noticed along the Samnite Apennines where, however, no relevant anomalies have been pointed out.

Nonetheless, the initial comparison of topographic anomalies with first-order geolithological units (Figure 2) and the anticorrelation pointed out in the relief profiles (SW1, SW3, SW4, and SW6 in Figure 5) yielded preliminary information useful to direct more advanced metrics.

The χ-z analysis, in fact, provided a more significant contribution to discriminate the possible lithological control on the anomalies (Figure 7(a)). The knickpoints we interpret having a tectonic origin (black stars in Figure 10) isolate stream reaches with a weak k_{sn} upstream increase (see Table 2). Nevertheless, most of the knickpoints cluster. A lack of lithologic control seems to be also supported in the peculiar setting of the Abruzzo Adriatic piedmont where the Middle Pleistocene conglomerates ("*Ripa Teatina*" conglomerates *auctorum* in [87, 88]) extensively crop out. Here, all the k_{sn} increases (see the Arielli, Moro, and Feltrino rivers—#5, #6, and #7 in Figures 6(a) and 7(a); upper right inset in Figure 10) fall within the older Plio-Pleistocene clayey units. The evidence diminishes ambiguity in the interpretation because the knickpoints fall in the same (less competent) rock type. The latter would unlikely be able to maintain small height differences over a long time if not related to the persistence of tectonically induced knickpoints.

The transient deviations from the theoretical profiles are achieved mostly along the smaller rivers, often through knickzones (Figure 7(b)) instead of isolated knickpoints.

Even if knickzones have been associated with base-level changes [154] or with alternations of lithology [155, 156], they have also been documented as a response to locally focused uplift [157, 158]. This scenario could fit with the evident clustering of knickpoints in the Adriatic piedmont area (Figure 10).

Approaching the mouth of the main rivers (Aterno-Pescara, Aventino-Sangro, Trigno, Biferno, and Fortore—#2, #8, #11, #13, and #15 in Figures 6(a) and 7(a)), evidence for differential uplift coming from the analysis of the geomorphic indices is lacking. Nevertheless, the morphotectonic analysis of the late Quaternary terraces along the northern bank of the Pescara river (#2 in Figures 6(a) and 8) suggests recent deformation along its lower course. The downstream convergence of the terrace treads (especially ACT and AVM1) and their disruption suggest that they underwent differential uplift and that this deformation is at least younger than the Middle Pleistocene (Figure 8(a)).

Moreover, even if the stream-power law does not apply where rivers exhibit alluvial conditions, it is worth noticing that the knickpoint highlighted along the Pescara river (1 km downstream of the Alanno dam—yellow star in Figures 7 and 10) is also located where terrace treads show the largest tilt (in Figure 8 and light blue strip in Figure 10). The deformation age suggested by the terrace analysis carried out along the Pescara river is younger than that inferred from the seismic line interpretation (Figure 9, traces also in Figure 2), where the youngest and slightly folded reflector is the TGe (1.8 Ma). This confirms, on the one hand, the weak resolution of commercial seismic lines in highlighting late Quaternary deformation. On the other hand, the thrust deformation highlighted on the western border of both the sections L1 and L2, even if not well defined for the Middle Pleistocene-to-Holocene successions, coincides with the sectors pointing out deformation along the Pescara terrace deposits (A to B in Figure 8). A possible explanation for this inconsistency has already been advanced for the NAOF- and CAOF-related thrust structures [8, 94]. In these cases, the lack of deformation affecting the middle-late Quaternary seismic reflectors has been interpreted as recording the effect of the large increase of sediment supply (in the Padanian and central Adriatic foredeep), during the Quaternary eustatic low stand. The interpretations of published seismic lines crossing the northern and central Adriatic foredeep ([80, 81] and this study) show comparable thicknesses of the Plio-Quaternary siliciclastic deposits for similar chronostratigraphic records. This evidence suggests that even in the study area, the noticeable sediment supply that eventually occurred in the Quaternary could have produced a smaller (apparent) fault throw along the easternmost thrusts. This would reconcile the lack of thrust deformation on seismic lines with the morphotectonic evidence of deformation pointed out in this study (Figure 8).

Due to the partitioning of the contractional deformation over the several splays of the CAOF-trailing imbricate (Figure 9), the amount of shortening associated with each fault could be too low to be detected at the shallowest levels, given the poor resolution capacity of the seismic lines.

5.2. Tectonic Implications of the Evidence of Uplift. Combining all the findings described here with the main structural elements known for the outer Abruzzo and Molise regions (Figure 10), we conclude that portions of the CAOF and SAOF (and related thrust structures) show variable evidence of tectonic-related deformation.

In the structural sketch of Figure 10, the deformation is ascribed to be accommodated along some of the buried structures reported (and slightly adapted) from the literature [16, 45, 56].

Most of the evidence of uplift is coincident with the hanging wall of the outer buried thrust structures facing the Abruzzo piedmont sector, especially along the NW-SE-trending Abruzzo Citeriore Basal Thrust (ACBT hereinafter, Figure 10), tentatively proposed in [50].

Along the ACBT and, in particular, in the Orsogna area (inset (a) in Figure 10), our evidence of uplift agrees with the preliminary hints of localized uplift provided in [46] and [48], which suggested the activation of the buried thrust at least since Middle Pleistocene times. This age agrees with that we argue for the Pescara terrace treads.

We propose localized uplift also along the Osento river (#9 in Figures 6(a) and 7(a)). The latter and the Sinello (#10 in Figure 6(a)) show deflections close to the coast, thus suggesting the possible growth of a fold that forced the rivers to flow to NW and SE, respectively. Along the same rivers, moving westward and uphill, the observed knickpoints could be ascribed to the activity of the thrusts related to the Casoli-(C-) Bomba (B) high [16, 42, 55].

The C-B high has been recognized in seismic lines from the eastern margin of the Majella Mt to the high Molise region (C and B in Figure 10, respectively) and is represented by NNW-SSE/N-S-trending popup-like structure whose time of incorporation, in the Apenninic mountain chain, is reported to be in the late Pliocene-Lower Pleistocene [14, 42]. Nevertheless, the development of the SW-NE drainage system in the Abruzzo region began in the upper part of the Middle Pleistocene [107, 130]; thus, the bending of the Aventino-Sangro river (#8 in Figure 6(a)), where it approaches the Adriatic piedmont, and the observed knickpoints (Figure 10) in the hanging wall of B, support the interpretation of a younger activation. This remark agrees with the bimodal topographic anomaly pointed out along the swath profile SW3 (Figures 4(a) and 5) and, again, with the terrace analysis proposed in [107]. In fact, it is worth noticing that B high is adjacent (along strike) to the terrace anomalies (see the light blue strips in Figure 10) signaled in [48] along one of the main tributaries of the Sangro river (i.e., the Aventino).

Northward, the thrust structures in B overlap with that leading C, east of the Majella Mt, and may account for the uplift highlighted by the knickpoints picked along the upper course of the Moro river (#6 in Figures 6(a), 7(a), 7(b), and 10) and for the relief anomalies pointed out along the swath profile SW6 (Figures 4(a) and 5). The latter also coincides with the alignment of the knickpoints observed along rivers #3 and #4 (Figures 6(a), 7(a), and 10), with the latter marked as doubtful. We are aware that the analysis of the geomorphic indices did not provide constrained evidence of

differential uplift in this sector. Nevertheless, the along-strike alignment of the knickpoints with the location of the terrace deformation along the Pescara river's lower course (Figures 8 and 10) suggests that despite the limitations to the analysis of river profiles, our observations support late Quaternary activity along the C-related thrust structures. This deformation may be equivalent and considered in association with that proposed for the southern strand of the CoS, as interpretable from the topographic anomaly observed along the swath profile SW1 (Figures 5 and 10) in association with the morphotectonic analysis carried out along the Pescara river (Figures 8 and 10).

No tectonic significance is attributable, in our opinion, to the (doubtful) knickpoints reported along the uppermost course of rivers #3 and #4. They likely coincide with additional lithological variations [85] within the limestones cropping out in the Majella massif (see also observations reported in Section 4.1).

The anomalies indicated from the relief and k_{sn} analyses southeast of Teramo, at the hanging wall of the Bellante-Cellino thrust (BCS in Figure 10), remain difficult to explain if we consider that only a (doubtful) knickpoint has been highlighted along the Saline river (#1 in Figure 6(a), Figures 7(a) and 10). Moreover, the deformation time of the BCS has been reported to stop in the late Pliocene (~2.5 Ma) ([95] and references therein). We do not have evidence for late Quaternary activity along the BCS. Further investigations are needed in this perspective.

Southward of the ACBT, in the Molise region, evidence of active deformation disappears. The lack of tectonic signals from the fluvial network analysis does not support the recent activity of the SAOF along the Frentani Mt front (outcropping front of the Apenninic thrust belt, *sensu* [45]). The isolated knickpoint which has been pointed out, upstream, along the Fortore river (Figures 7(a) and 10) is not spatially related to any other anomaly and is located in a rearward position with respect to the SAOF. Similar remarks can be raised for the Saccione river (#14 in Figures 6(a), 7(a), and 10) which is located, on the contrary, in a forward position with respect to the SAOF leading edge. Possible local-scale alternation of lithologies could account for these anomalies. On the other hand, the increase in the local relief between 25 and 45 km along SW4 (Figures 4(a) and 5) cannot support, alone, tectonic uplift. Our outcomes in the Molise region agree with those provided in [104] which reported, between the Trigno and Fortore rivers (#11 and #15 in Figure 6(a), respectively), no evidence of thrust deformation later than the upper part of the Early Pleistocene.

On the whole, our approach aimed to test for late Quaternary activity along the Apenninic Outer Front provides hints in the Abruzzo region (and locally) supporting the working hypothesis, with some limitations deriving from the unsuitability of the stream power law along the big rivers flowing in the study area (see Section 4.2.1). We recognize that the evidence along the CoS and the ACBT, as well as along the C and B thrusts, is not always strong and has some ambiguity because of the noticeable variability of the rock-type outcrops and low-magnitude anomalies. Nevertheless, the different methods suggest disequilibrium conditions coinciding with shortening-related structures that are already known (or inferred) to be seismogenic (i.e., CoS and ACBT). The along-strike clustering of the anomalies strengthens their attribution to late Quaternary active shortening.

Our findings of localized shortening-related uplift are in line with some of the recent literature which, exploiting seismological, geophysical, and/or morphotectonic analyses, conclude that shortening at the boundary between the central and southern Apennines can be possibly accommodated by seismogenic faults [48, 51, 168, 169]. Differently, they are difficult to explain with long-wavelength regional uplift eventually related to dynamic processes (see [127] among the others; see Section 2.1 for more extensive literature) in the central-southern Apennines.

5.3. Seismotectonic Considerations. The results presented in this study compel consideration for the seismotectonic setting of the Abruzzo and Molise regions' outer sectors. In instrumental times, both the offshore CAOF and CoS (Figure 10) have been only characterized by sparse, low-to-moderate seismicity (Mw 4.5-5.5) [1]. The most recent event affecting the ABT in the study area was the Mw 5.1 Porto San Giorgio, 1987 reverse upper-crust earthquake ([159]; Figure 11(b), 1).

On the other hand, the ACBT and its hanging wall structures have been characterized by a substantial lack of background seismicity (Figure 11(b), 1) [167, 170, 171]. Nevertheless, an association of the SW-dipping ACBT or even its backthrust with the 1706 (Mw 6.8) and 1933 (Mw 5.9) historical earthquakes (see the geological section and the macroseismic epicenters in Figures 11(a) and 11(b), respectively) has been suggested [9, 49, 51]. Furthermore, the lack of energetic events could be the consequence of the low strain rates related to thrust mechanisms in Italy [51], the latter having characteristic recurrence about three times larger (~2000 y) than those with normal mechanisms.

Even if the study area does not display energetic seismicity [4, 172], the available focal mechanisms of the few events located east of the intra-Apennines extensional domain (Figure 11(b), 1) exhibit reverse/transpressive kinematics (from [5, 159–167]).

Their focal depth increases westward, coherently with the geometry of a basal west-dipping thrust plane. Some minor events (maximum magnitude Mw = 3.4, October 11, 2008) show focal plane trends which are coherent with the geometry of the Casoli-Bomba structures. Their sense of motion and that of the focal mechanisms falling in the Abruzzo region (and to the north) agree with the velocity field provided in [6] (see profile H-H' in Figure 11(b), 2) and with the compressional domain of the seismotectonic zonation proposed in [168] (red strip in Figure 11(b), 2). The agreement between the approximate 1.6 mm/y slip rate we proposed in the Pescara sector (averaged over the Late Pleistocene) and the value reported in [6] (~2 mm/y) further supports our seismotectonic interpretation. Finally, the focal mechanisms exhibit an average maximum shortening (P) axis which is 244/05 trending (inset in Figure 11(b), 1). The latter is perpendicular to the ACBT

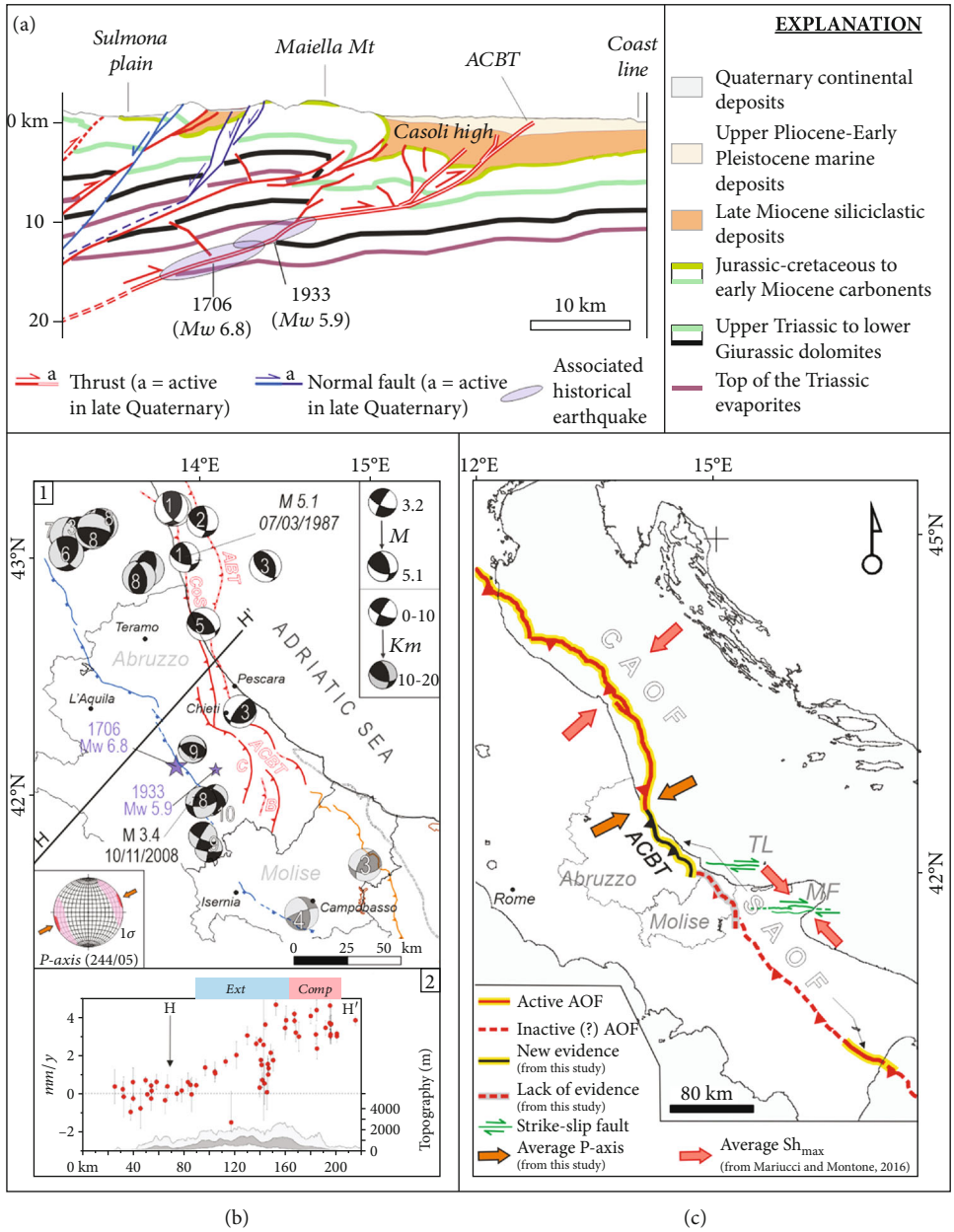

Figure 11: Regional and seismotectonic implications of the localized rock uplift highlighted in the Abruzzo region. (a) Interpretative geological section (trace in Figure 10) across the Majella massif and the Abruzzo Citeriore Basal Thrust (ACT) (from [50, 96]) showing the inferred geometry of the active Abruzzo SAOF section (Abruzzo Citeriore Basal Thrust) and of the Casoli thrust (at its hanging wall). The 1706 and 1933 associated historical earthquakes are reported as proposed in [49] (the respective macroseismic epicenters—stars—are in (b), 1). (b) (1) Focal mechanisms available for the sector from the following: 1: [159]; 2: [160]; 3: [161]; 4: [162]; 5: [163]; 6: [5]; 7: [164]; 8: [165]; 9: [166]; 10: [167]. Epicenters of the historical earthquakes (purple stars) associated with shortening deformation (from [49]) are also reported. Thrust and normal fault key as in Figure 10. In the lower-left inset, the average *P*-axis as derived from the focal mechanisms (Abruzzo region and northward) has been reported. (2) GPS velocity data along the section H-H' crossing the Apenninic belt (Eurasian-fixed frame, redrawn from [6]) and comparison with the sectors experiencing extension and compression (light blue and red strips, respectively) according to the seismotectonic zonation provided in [168]. (c) Newly identified late Quaternary active segment of the Southern Apenninic Outer Front (SAOF) and its inferred structural-kinematic correlation with the Central Apenninic Outer Front (CAOF).

in Abruzzo (Figure 11(c)) and agrees with the average Sh$_{max}$-axes along the CAOF, to the north ([4], as in Figure 1).

The two focal mechanisms in the Molise region (transparent color-coded), and their depth, are consistent with the dextral strike-slip sense of motion (e.g., the Mattinata fault and Tremiti line—MF and TL in Figure 11(c), respectively) in the foreland of the Apenninic belt system [94, 173, 174]. The possible connection of the MF with deep seismogenic strike-slip structures, beneath the Molise axial part

of the Apennines, has been suggested [175–177]. Interaction of the SAOF with the foreland strike-slip system would account for the lack of clear evidence of shortening in Molise. New detailed dating of the late Quaternary continental deposits could ease the application of morphotectonic analysis along the main river of the region. This would provide, as in the Pescara river case, new hints supporting or further invalidating the hypothesis of the late Quaternary SAOF activity for that area.

The structural connection (in the Abruzzo region) between ABT and ACBT, as well as between the structures at their hanging wall (CoS, C, and B), is possible, despite discontinuous evidence between the different segments (Figure 10). The seismogenic attitude of both ABT and CoS, to the north, and the structural alignment between these thrusts and the anomalies pointed out to the southeast lead to this interpretation. The discontinuous signals from the topography and fluvial network could be equally explained as the activation, during the time (late Quaternary) of different segments rather than a continuous structural element, or as being the result of incomplete signals of uplift [178].

6. Conclusions

In this paper, we inspected the hypothesis of late Quaternary active shortening in central-southern Italy along the SAOF and its connection with the CAOF. We exploited in the Abruzzo and Molise regions a combined relief, fluvial network, and late Quaternary landform analysis aimed at assessing evidence of uplift consistent with compressional tectonics.

The results highlight localized uplift along the Abruzzo Adriatic piedmont and its inner foothill sector. No clear evidence of uplift has been observed in the Molise region.

The multidisciplinary approach allowed us to exclude in some sectors (e.g., along the Adriatic piedmont) the exclusive lithological influence on the observed anomalies that can be explained with concurrent active shortening along the ACBT arcuate segment (SAOF, in southern Abruzzo, Figures 11(b) and 11(c)). Analogously, in the foothill sector, evidence of uplift has been tentatively associated with the C and B thrust structures and, toward the north, to the CoS (ACBT and CAOF hanging walls, respectively).

More robust constraints on the late Quaternary activity of the SAOF in Abruzzo come from the differential uplift observed along the Pescara terrace treads. This deformation is difficult to explain with long-wavelength regional uplift alone and further supports the hypothesis of compressional tectonics throughout the Middle and Late Pleistocene. Possible ongoing deformation is based on seismicity and historical earthquakes.

Our approach proved challenging to test evidence of deformation in an area characterized by low deformation rates. However, our results and interpretations fit with the recent literature and the seismotectonic setting of the sector and suggest the need to reconsider, in terms of seismic hazard assessment, the possible existence of seismogenic structures along the Apenninic Outer Front in central-southern Italy.

Data Availability

Tables embedded in the paper, as well as the new vector data (shapefiles-ESRI format) produced, interpreted, and used to support the findings of this study, have been made accessible in Federica Ferrarini, J Ramón Arrowsmith, Francesco Brozzetti, Rita de Nardis, Daniele Cirillo, Kelin X Whipple, and Giusy Lavecchia (2021). COLOSSEO-1 [data set]. Zenodo. doi:10.5281/zenodo.4729624.

Additional Points

Resources. The seismic lines presented in this study have been managed and in-depth converted using the MOVE Suite Software (vers. 2019.1) by Petroleum Experts Ltd., Edinburgh, Scotland, UK (https://www.petex.com/products/move-suite/). The geomorphic indices and the fluvial network features have been computed using the MATLAB-based software: TopoToolbox [131, 132] and Topographic Analysis Kit (TAK) for TopoToolbox [133]. Lidar data have been provided by the Italian Ministry of the Environment (http://www.pcn.minambiente.it/mattm/en/tag/dati-lidar-en/). All vector data have been stored and managed in a georeferenced database using ArcMap (by ESRI, v. 10.6.1). The final editing of figures has been carried out using the CorelDRAW Graphics Suite (v. 2020). All names of epochs/series rely on the chronostratigraphic chart reported in [179, 180].

Conflicts of Interest

The authors declare that they have no conflicts of interest.

Funding

This work is part of the "COLOSSEO" research project that has received funding from the European Union's Horizon 2020 research and innovation programme, under Grant Agreement #795396.

Acknowledgments

We are grateful to thank Manfred Strecker for the critical review of the morphotectonic signatures of compressional deformation and to Vito Bracone and Pietro Aucelli for the useful discussions that helped to frame the Molise tectonostratigraphic setting within the regional context of the Apenninic Outer Front. We also thank the Editor and the reviewers for their valuable comments which helped to improve the original manuscript.

Supplementary Materials

Supplementary 1. Supplementary Materials S1 Pescara (along-river) late Quaternary deposits. In this table, we report a more detailed description of the middle-late Quaternary deposits, cropping out along the Pescara river, as reported in the available maps at 1 : 50,000 scale and related explanatory notes (CARG project [87, 88]). We used the outcrops of these deposits, in combination with high-

resolution topography, to extract the fluvial terrace tread heights and to investigate their morphotectonic setting along the Pescara river longitudinal profile (see for details Section 3.4 of the paper). For the references, we relate the reader to the main text.

Supplementary 2. Supplementary Materials S2 Slope-area regressions and related concavity index (θ) (see also Table 1) computed for each river investigated in this study. In the location map, the color-coded drainage basins are reported. Key: 1: Saline; 2: Aterno-Pescara; 3: Alento; 4: Foro; 5: Arielli; 6: Moro; 7: Feltrino; 8: Aventino-Sangro; 9: Osento; 10: Sinello; 11: Trigno; 12: Sinarca; 13: Biferno; 14: Saccione; 15: Fortore.

Supplementary 3. Supplementary Materials S3 Sensitivity test of the concavity index. We tested how using a different critical area could affect the concavity index (θ) computation and the χ-transformed along-river analysis. We used in this test $A_{crit} = 1\,km^2$ (in comparison to the $A_{crit} = 0.1\,km^2$ used for the computation reported in the paper) to make regression of log *S*-log *A* and compute the concavity index θ for some of the rivers analyzed in this study. In particular, we performed this analysis for some of the rivers which exhibited higher (e.g., Arielli, Moro, and Feltrino—#5, #6, and #7 in the paper) and lower values (Aterno-Pescara and Aventino-Sangro—#2 and #8 in the paper) with respect to the average concavity index ($\theta = 0.36$) used in the work (see Table 2). We demonstrate that even if the concavity index of each river slightly varies (using $A_{crit} = 1\,km^2$), the location and meaning (tectonic vs. stratigraphic or decreasing k_{sn}) of the knickpoints along the rivers are not affected (see also Supporting Material S6 for comparison). In panels 1 to 5, we report the θ values resulting from the new log *S*-log *A* regressions. In panels 6 to 10, we annex images showing the procedure used for the k_{sn} regression carried out to identify knickpoints over the transformed river profiles (χ-*z* plots) and implemented using the "KsnProfiler" TAK function [133]. We used for each river the concavity index (θ) computed using $A_{crit} = 1\,km^2$ (see panels 1-5). The residuals obtained from each computation are also reported (see for comparison supplementary information S6). As further confirmation that the location and meaning (tectonic vs. stratigraphic or decreasing k_{sn}) of the knickpoints along the rivers are not affected by a different A_{crit} value, we show in panel 11 (same frame as in Figure 10(a) of the paper) the location of the knickpoints obtained using different A_{crit} values ($A_{crit} = 0.1\,km^2$; $A_{crit} = 1\,km^2$).

Supplementary 4. Supplementary Materials S4 Seismic line (original) PEF-08-87. In panel 1, we report the paper copy of the seismic line PEF-08-87 (https://www.videpi.com/deposito/videpi/allegati/2976.pdf, in Figure 9 of the paper named L1) as available from [134] and which we interpreted and in-depth converted using the MOVE Suite Software by Petroleum Experts Ltd. (see Resources).

Supplementary 5. Supplementary Materials S5 Seismic line (original) PES-07. In panel 1, we report the paper copy of the seismic line PES-07 (https://www.videpi.com/deposito/videpi/sismicatitoli/all%203_Linea_PES-7.pdf, in Figure 9 of the paper named L2) as available from [134] and which we interpreted and in-depth converted using the MOVE Suite Software by Petroleum Experts Ltd. (see Resources).

Supplementary 6. Supplementary Materials S6 Transformed river profiles (χ-*z* plots) and knickpoint detection procedure for the rivers (#1 to #15) investigated in this study. We annex images showing the procedure used for the k_{sn} regression carried out to identify knickpoints over the transformed river profiles (χ-*z* plots) and implemented using the "KsnProfiler" TAK function ([133]; see references in the main text). For each of the rivers, we provide 2 panels with captions reporting the following: "stream_fits_# - name" and "stream_rsds_# - name," where "#" corresponds to the river number (as in Figure 6(a) of the paper) and "name" is the river name (see caption of Figure 6). In the panels, "stream_fits_# - name" are reported in the following order (from top to bottom): the χ-*z* plot with the segments chosen (black lines) for the calculation of best-fit k_{sn}; the auto k_{sn} computation within the picked segments; the river longitudinal profile; and the slope-area plot. The averaged k_{sn} values computed for each picked segment (and over each river) and interpreted (tectonic vs. stratigraphic) in our analysis are also reported in Table 2 of the paper. In the images, "stream_rsds_# - name" are reported the plots of the residuals on the k_{sn} fit that the function also produces for each river.

References

[1] M. Locati, R. Camassi, B. Lolli, and P. Gasperini, *Italian Parametric Earthquake Catalogue (CPTI15), version 2.0*, Istituto Nazionale di Geofisica e Vulcanologia (INGV), 2019.

[2] G. Lavecchia, F. Brozzetti, M. Barchi, M. Menichetti, and J. V. A. Keller, "Seismotectonic zoning in east-central Italy deduced from an analysis of the Neogene to present deformations and related stress fields," *Geological Society of America Bulletin*, vol. 106, no. 9, pp. 1107–1120, 1994.

[3] C. Chiarabba and P. de Gori, "The seismogenic thickness in Italy: constraints on potential magnitude and seismic hazard," *Terra Nova*, vol. 28, no. 6, pp. 402–408, 2016.

[4] P. Montone and M. T. Mariucci, "The new release of the Italian contemporary stress map," *Geophysical Journal International*, vol. 205, no. 3, pp. 1525–1531, 2016.

[5] F. Visini, R. de Nardis, and G. Lavecchia, "Rates of active compressional deformation in central Italy and Sicily: evaluation of the seismic budget," *International Journal of Earth Sciences*, vol. 99, Supplement 1, pp. 243–264, 2010.

[6] R. Devoti, N. D'Agostino, E. Serpelloni et al., "A combined velocity field of the Mediterranean region," *Annals of Geophysics*, vol. 60, no. 2, 2017.

[7] M. M. C. Carafa and P. Bird, "Improving deformation models by discounting transient signals in geodetic data: 2. Geodetic data, stress directions, and long-term strain rates in Italy," *Journal of Geophysical Research (Solid Earth)*, vol. 121, no. 7, pp. 5557–5575, 2016.

[8] G. Pezzo, L. Petracchini, R. Devoti et al., "Active fold-thrust belt to foreland transition in northern Adria, Italy, tracked by seismic reflection profiles and GPS offshore data," *Tectonics*, vol. 39, no. 11, 2020.

[9] DISS Working Group, *Database of Individual Seismogenic Sources (DISS), version 3.2.1: a compilation of potential sources for earthquakes larger than M 5.5 in Italy and surrounding areas*, Istituto Nazionale di Geofisica e Vulcanologia, 2018, http://diss.rm.ingv.it/diss/.

[10] A. Govoni, A. Marchetti, P. de Gori et al., "The 2012 Emilia seismic sequence (Northern Italy): imaging the thrust fault system by accurate aftershock location," *Tectonophysics*, vol. 622, pp. 44–55, 2014.

[11] G. Lavecchia, R. de Nardis, G. Costa et al., "Was the Mirandola thrust really involved in the Emilia 2012 seismic sequence (northern Italy)? Implications on the likelihood of triggered seismicity effects," *Bollettino di Geofisica Teorica ed Applicata*, vol. 56, pp. 461–488, 2015.

[12] M. Boccaletti, N. Ciaranfi, D. Cosentino et al., "Palinspastic restoration and paleogeographic reconstruction of the peri-Tyrrhenian area during the Neogene," *Palaeogeography, Palaeoclimatology, Palaeoecology*, vol. 77, no. 1, pp. 41–IN13, 1990.

[13] P. Casero, "Structural setting of petroleum exploration palys in Italy," in *Special Volume of the Italian Geological Society for the 32th IGC*, Florence, 2004.

[14] E. Patacca and P. Scandone, "The Plio-Pleistocene thrust belt – foredeep system in the southern Apennines and Sicily (Italy)," in *Special Volume of the Italian Geological Society for the IGC 32*, pp. 93–129, Florence, 2004.

[15] D. Cosentino, P. Cipollari, P. Marsili, and D. Scrocca, "Geology of the central Apennines: a regional review," *Journal of the Virtual Explorer*, vol. 36, 2010.

[16] CNR, *Structural Model of Italy, Progetto Finalizzato Geodinamica S.P., 5: Quaderni de La Ricerca Scientifica, 114, sheet 4, scale 1:500,000*, S.E.L.CA., Firenze, 1992.

[17] L. C. Benedetti, P. Tapponnier, Y. Gaudemer, I. Manighetti, and J. van der Woerd, "Geomorphic evidence for an emergent active thrust along the edge of the Po Plain: the Broni-Stradella fault," *J Geophys. Res.*, vol. 108, no. B5, p. 2238, 2003.

[18] A. Michetti, F. Giardina, F. Livio et al., "Active compressional tectonics, Quaternary capable faults, and the seismic landscape of the Po Plain (northern Italy)," *Annals of Geophysics*, vol. 55, no. 5, pp. 969–1001, 2013.

[19] F. E. Maesano, C. D'Ambrogi, P. Burrato, and G. Toscani, "Slip-rates of blind thrusts in slow deforming areas: examples from the Po Plain (Italy)," *Tectonophysics*, vol. 643, pp. 8–25, 2015.

[20] M. Boccaletti, G. Corti, and L. Martelli, "Recent and active tectonics of the external zone of the Northern Apennines (Italy)," *Int J Earth Sci (Geol Rundsch)*, vol. 100, no. 6, pp. 1331–1348, 2011.

[21] A. Ponza, F. J. Pazzaglia, and V. Picotti, "Thrust-fold activity at the mountain front of the Northern Apennines (Italy) from quantitative landscape analysis," *Geomorphology*, vol. 123, no. 3-4, pp. 211–231, 2010.

[22] V. Picotti and F. J. Pazzaglia, "A new active tectonic model for the construction of the Northern Apennines mountain front near Bologna (Italy)," *Journal of Geophysical Research*, vol. 113, no. B8, p. B08412, 2008.

[23] K. W. Wegmann and F. J. Pazzaglia, "Late Quaternary fluvial terraces of the Romagna and Marche Apennines, Italy: climatic, lithologic, and tectonic controls on terrace genesis in an active orogen," *Quaternary Science Reviews*, vol. 28, no. 1-2, pp. 137–165, 2009.

[24] G. Lavecchia, P. Boncio, and N. Creati, "A lithospheric-scale seismogenic thrust in central Italy," *Journal of Geodynamics*, vol. 36, no. 1-2, pp. 79–94, 2003.

[25] G. Lavecchia, R. De Nardis, F. Visini, F. Ferrarini, and M. S. Barbano, "Seismogenic evidence of ongoing compression in eastern-central Italy and mainland Sicily: a comparison," *Italian Journal of Geosciences (Bollettino della Società Geologica Italiana)*, vol. 126, pp. 209–222, 2007.

[26] E. Battimelli, G. M. Adinolfi, O. Amoroso, and P. Capuano, "Seismic activity in the central Adriatic offshore of Italy: a review of the 1987 ML 5 Porto San Giorgio earthquake," *Seismological Research Letters*, vol. 90, pp. 1889–1901, 2019.

[27] J. C. Bousquet and G. Lanzafame, "Quaternary compressive deformation on the southern edge of the Etna volcano (Sicily). Comptes rendus de l'Académie des sciences. Série II. Mechanics. Physics. Chemistry. Space sciences," *Earth sciences*, vol. 303, pp. 235–240, 1986.

[28] G. Lanzafame, M. Neri, M. Coltelli, L. Lodato, and D. Rust, "North–south compression in the Mt. Etna region (Sicily): spatial and temporal distribution," *Acta Vulcanologica*, vol. 9, pp. 121–133, 1997.

[29] S. Carbone, S. Catalano, A. Di Stefano, P. Guarnirei, and F. Lentini, "Evoluzione tettonica della Sicilia orientale," in *Le ricerche del GNDT nel campo della pericolosità sismica (1996–99)*, F. Galadini, C. Meletti, and A. Rebez, Eds., pp. 39–44, CNR-Gruppo Nazionale per la Difesa Terremoti, Roma, 2000.

[30] C. Monaco, M. Bianca, S. Catalano, G. De Guidi, and L. Tortorici, "Sudden change in the Late Quaternary tectonic regime in eastern Sicily: evidences from geological and geomorphological features," *Bollettino della Società Geologica Italiana*, vol. 1, pp. 901–913, 2002.

[31] S. Catalano, S. Torrisi, and C. Ferlito, "The relationship between Late Quaternary deformation and volcanism of Mt. Etna (eastern Sicily): new evidence from the sedimentary substratum in the Catania region," *Journal of Volcanology and Geothermal Resesarch*, vol. 132, no. 4, pp. 311–334, 2004.

[32] M. Grasso, G. Ciuccio, R. Maniscalco, P. Garofano, F. La Manna, and R. Stamilla, "Plio-Pleistocene structural evolution of the western margin of the Hyblean Plateau and the Maghrebian foredeep, SE Sicily. Implications for deformational history of the Gela Nappe," *Ann. Tecton*, vol. IX, pp. 7–21, 1995.

[33] L. Torelli, M. Grasso, G. Mazzoldi, and D. Peis, "Plio-Quaternary tectonic evolution and structure of the Catania foredeep, the northern Hyblean Plateau and the Ionian shelf (SE Sicily)," *Tectonophysics*, vol. 298, no. 1-3, pp. 209–221, 1998.

[34] C. Monaco, S. Mazzoli, and L. Tortorici, "Active thrust tectonics in western Sicily (Southern Italy): the 1968 Belice earthquake sequence," *Terra Nova*, vol. 8, no. 4, pp. 372–381, 1996.

[35] S. Catalano, G. De Guidi, G. Lanzafame et al., "Inversione tettonica positive Tardo-Quaternaria nel Plateau Ibleo (Sicilia SE)," *Rendiconti della Società Geologica Italiana*, vol. 2, pp. 118–120, 2006.

[36] G. de Guidi, S. Imposa, S. Scudero, and M. Palano, "New evidence for Late Quaternary deformation of the substratum of Mt. Etna volcano (Sicily, Italy): clues indicate active crustal doming," *Bulletin of Volcanology*, vol. 76, no. 5, p. 816, 2014.

[37] G. Lavecchia, F. Ferrarini, R. de Nardis, F. Visini, and M. S. Barbano, "Active thrusting as a possible seismogenic source in Sicily (Southern Italy): Some insights from integrated

structural-kinematic and seismological data," *Tectonophysics*, vol. 445, no. 3-4, pp. 145–167, 2007.

[38] T. Sgroi, R. de Nardis, and G. Lavecchia, "Crustal structure and seismotectonics of central Sicily (southern Italy): new constraints from instrumental seismicity," *Geophysical Journal International*, vol. 189, no. 3, pp. 1237–1252, 2012.

[39] A. Polonia, L. Torelli, P. Mussoni, L. Gasperini, A. Artoni, and D. Klaeschen, "The Calabrian arc subduction complex in the Ionian Sea: regional architecture, active deformation, and seismic hazard," *Tectonics*, vol. 30, no. 5, 2011.

[40] L. Ferranti, E. Santoro, M. E. Mazzella, C. Monaco, and D. Morelli, "Active transpression in the northern Calabria Apennines, southern Italy," *Tectonophysics*, vol. 476, no. 1-2, pp. 226–251, 2009.

[41] R. Caputo, M. Bianca, and R. D'Onofrio, "Ionian marine terraces of southern Italy: insights into the Quaternary tectonic evolution of the area," *Tectonics*, vol. 29, no. 4, article TC4005, 2010.

[42] E. Patacca, P. Scandone, M. Bellatalla, N. Perilli, and U. Santini, *La zona di giunzione tra l'arco appenninico settentrionale e l'arco appenninico meridionale nell'Abruzzo e nel Molise: Studi geologici camerti, Special Volume "Studi preliminari all'acquisizione dati del profilo CROP 11 Civitavecchia-Vasto" (1991/1992)*, pp. 417–441, 1992.

[43] P. Casero, F. Rowe, L. Endignoux et al., "Neogene geodynamic evolution of the Southern Apennines," *Memorie della Societa Geologica Italiana*, vol. 41, pp. 109–120, 1992.

[44] A. Pizzi, "Plio-Quaternary uplift rates in the outer zone of the central Apennines fold-and-thrust belt, Italy," *Quaternary International*, vol. 101–102, pp. 229–237, 2003.

[45] L. Vezzani, A. Festa, and F. C. Ghisetti, "Geology and tectonic evolution of the central-southern Apennines, Italy," *Geological Society of America, Special Paper*, vol. 469, pp. 1–58, 2010.

[46] G. Pomposo and A. Pizzi, "Evidenze di tettonica recente ed attiva nel settore esterno sepolto dell'Appennino centrale abruzzese," *Rendiconti online Società Geologica Italiana*, vol. 5, pp. 176–178, 2009.

[47] F. Ferrarini, J. R. Arrowsmith, F. Brozzetti, D. Cirillo, R. de Nardis, and G. Lavecchia, "Late-Quaternary tectonics along the peri-Adriatic belt of central Italy: possible evidence of active shortening from topography, fluvial network analysis, and landscape evolution," *Geological Society of America Annual Meeting, Abstracts with Programs*, vol. 51, no. 5, 2019.

[48] S. Racano, G. Fubelli, E. Centamore, M. Bonasera, and F. Dramis, "Geomorphological detection of surface effects induced by active blind thrusts in the southern Abruzzi peri-Adriatic belt (Central Italy)," *Geografia Fisica e Dinamica Quaternaria*, vol. 43, pp. 3–13, 2020.

[49] G. Lavecchia, and R. de Nardis, *Seismogenic sources of major earthquakes of the Maiella area (central Italy): constraints from macroseimic field simulations and regional seimotectonics*, Convegno annuale dei progetti sismologici, Convenzione-Quadro tra Dipartimento della Protezione Civile e Istituto Nazionale di Geofisica e Vulcanologia–Triennio 2007-09, Rome, Italy, 2009.

[50] G. Lavecchia, R. de Nardis, D. Di Naccio, F. Ferrarini, D. Cirillo, and F. Brozzetti, "Active compression in Eastern Abruzzo (central Italy): evidences from geological morphotectonic and macroseismic data analyses," *Rendiconti Online Società Geolica Italiana*, vol. 36, 2015.

[51] F. Riguzzi, M. Crespi, R. Devoti, C. Doglioni, G. Pietrantonio, and A. R. Pisani, "Strain rate relaxation of normal and thrust faults in Italy," *Geophysical Journal International*, vol. 195, no. 2, pp. 815–820, 2013.

[52] P. Galli and F. Pallone, "Reviewing the intensity distribution of the 1933 earthquake (Maiella, Central Italy): clues on the seismogenic fault," *Alpine and Mediterranean Quaternary*, vol. 32, pp. 93–100, 2019.

[53] F. Mostardini, S. Merlini, and Appennino, "Centro-meridionale. Sezioni geologiche e proposta di modello strutturale," *Memorie della Società Geologica Italiana*, vol. 35, pp. 177–202, 1986.

[54] A. M. Noguera and G. Rea, "Deep structure of the Campanian-Lucanian Arc (Southern Apennine, Italy)," *Tectonophysics*, vol. 324, no. 4, pp. 239–265, 2000.

[55] E. Patacca and P. Scandone, "Geology of the Southern Apennines," in *Results of the CROP Project Sub-project CROP-04 Southern Apennines (Italy): Italian Journal of Geosciences (Bollettino della Società Geologica Italiana)*, A. Mazzotti, E. Patacca, and P. Scandone, Eds., vol. 7 of Special Issue, pp. 75–119, 2007.

[56] E. Patacca, P. Scandone, E. di Luzio, G. P. Cavinato, and M. Parotto, "Structural architecture of the central Apennines: interpretation of the CROP 11 seismic profile from the Adriatic coast to the orographic divide," *Tectonics*, vol. 27, no. 3, p. TC3006, 2008.

[57] G. Toscani, P. Burrato, D. Di Bucci, S. Seno, and G. Valensise, "Plio-Quaternary tectonic evolution of the Northern Apennines thrust fronts (Bologna-Ferrara section, Italy): seismotectonic implications," *Bollettino della Società Geologica Italiana (Italian Journal of Geosciences)*, vol. 128, pp. 605–613, 2009.

[58] B. Trionfera, A. Frepoli, G. de Luca, P. de Gori, and C. Doglioni, "The 2013–2018 Matese and Beneventano seismic sequences (central–southern Apennines): new constraints on the hypocentral depth determination," *Geosciences*, vol. 10, no. 1, p. 17, 2020.

[59] D. W. Burbank, "Causes of recent Himalayan uplift deduced from deposited patterns in the Ganges Basin," *Nature*, vol. 357, no. 6380, pp. 680–683, 1992.

[60] D. R. Montgomery, "Slope distributions, threshold hillslopes, and steady-state topography," *American Journal of Science*, vol. 301, pp. 432–454, 1994.

[61] K. X. Whipple, E. Kirby, and S. H. Brocklehurst, "Geomorphic limits to climate-induced increases in topographic relief," *Nature*, vol. 401, no. 6748, pp. 39–43, 1999.

[62] E. Kirby and K. X. Whipple, "Expression of active tectonics in erosional landscapes," *Journal of Structural Geology*, vol. 44, pp. 54–75, 2012.

[63] P. Molin, F. J. Pazzaglia, and F. Dramis, "Geomorphic expression of active tectonics in a rapidly-deforming forearc, Sila Massif, Calabria, southern Italy," *American Journal of Science*, vol. 304, no. 7, pp. 559–589, 2004.

[64] R. A. DiBiase, K. X. Whipple, A. M. Heimsath, and W. B. Ouimet, "Landscape form and millennial erosion rates in the San Gabriel Mountains, CA," *Earth and Planetary Science Letters*, vol. 289, pp. 134–144, 2010.

[65] N. Rebai, T. Slama, M. M. Turki, M. B. Chelbi, H. Achour, and S. Bouaziz, "DEM-based calculation of residual topography: application to the Quaternary salt dome tectonics in Northern Tunisia," in *Vertical Geology Conference*, Lausanne, Switzerland, 2014.

[66] J. M. Azañón, J. P. Galve, J. V. Pérez-Peña et al., "Relief and drainage evolution during the exhumation of the Sierra Nevada (SE Spain): is denudation keeping pace with uplift?," *Tectonophysics*, vol. 663, pp. 19–32, 2015.

[67] J. Liu-Zeng, P. Tapponnier, Y. Gaudemer, and L. Ding, "Quantifying landscape differences across the Tibetan plateau: implications for topographic relief evolution," *Journal of Geophysical Research*, vol. 113, article F04018, 2008.

[68] P. England and P. Molnar, "Surface uplift, uplift of rocks, and exhumation of rocks," *Geology*, vol. 18, pp. 1173–1177, 1990.

[69] E. Kirby and K. Whipple, "Quantifying differential rock-uplift rates via stream profile analysis," *Geology*, vol. 29, pp. 415–418, 2001.

[70] C. Wobus, K. X. Whipple, E. Kirby et al., "Tectonics from topography: procedures, promise, and pitfalls," *Tectonics, Climate, and Landscape Evolution: Geological Society of America, Special Paper*, S. D. Willett, N. Hovius, M. T. Brandon, and D. M. Fisher, Eds., vol. 398, pp. 55–74, 2006.

[71] A. C. Whittaker, "How do landscapes record tectonics and climate?," *Lithosphere*, vol. 4, pp. 160–164, 2012.

[72] S. D. Willett, S. W. McCoy, J. T. Perron, L. Goren, and C. Chen, "Dynamic reorganization of river basins," *Science*, vol. 343, p. 1248765, 2014.

[73] A. Pedrera, J. V. Pérez-Peña, J. Galindo-Zaldívar, J. M. Azañón, and A. Azor, "Testing the sensitivity of geomorphic indices in areas of low-rate active folding (eastern Betic Cordillera, Spain)," *Geomorphology*, vol. 105, pp. 218–231, 2009.

[74] G. I. Marliyani, J. R. Arrowsmith, and K. X. Whipple, "Characterization of slow slip rate faults in humid areas: Cimandiri fault zone, Indonesia," *Journal of Geophysical Research Earth Surface*, vol. 121, pp. 2287–2308, 2016.

[75] D. Ntokos, E. Lykoudi, and T. Rondoyanni, "Geomorphic analysis in areas of low-rate neotectonic deformation: South Epirus (Greece) as a case study," *Geomorphology*, vol. 263, pp. 156–169, 2016.

[76] D. Cunningham, S. Grebby, K. Tansey, A. Gosar, and V. Kastelic, "Application of airborne LiDAR to mapping seismogenic faults in forested mountainous terrain, southeastern Alps, Slovenia," *Geophysical Research Letters*, vol. 33, article L20308, 2006.

[77] H. Kondo, S. Toda, K. Okumura, K. Takada, and T. Chiba, "A fault scarp in an urban area identified by LiDAR survey: a case study on the Itoigawa-Shizuoka tectonic line, central Japan," *Geomorphology*, vol. 101, pp. 731–739, 2008.

[78] O. Zielke and J. R. Arrowsmith, "LaDiCaoz and LiDARimager—MATLAB GUIs for LiDAR data handling and lateral displacement measurement," *Geosphere*, vol. 8, pp. 206–221, 2012.

[79] O. Zielke, Y. Klinger, and J. R. Arrowsmith, "Fault slip and earthquake recurrence along strike-slip faults — contributions of high-resolution geomorphic data," *Tectonophysics*, vol. 638, pp. 43–62, 2014.

[80] R. Fantoni and R. Franciosi, "Tectono-sedimentary setting of the Po Plain and Adriatic foreland," *Rendiconti Lincei. Scienze Fisiche e Naturali*, vol. 21, pp. S197–S209, 2010.

[81] P. Casero and S. Bigi, "Structural setting of the Adriatic basin and the main related petroleum exploration plays," *Marine and Petroleum Geology*, vol. 42, pp. 135–147, 2013.

[82] A. Artoni, "The Pliocene-Pleistocene stratigraphic and tectonic evolution of the central sector of the Western Periadriatic Basin of Italy," *Marine and Petroleum Geology*, vol. 42, pp. 82–106, 2013.

[83] S. Bigi, A. Conti, P. Casero, L. Ruggiero, R. Recanati, and L. Lipparini, "Geological model of the central Periadriatic basin (Apennines, Italy)," *Marine and Petroleum Geology*, vol. 42, pp. 107–121, 2013.

[84] R. Tinterri and L. Lipparini, "Seismo-stratigraphic study of the Plio-Pleistocene foredeep deposits of the Central Adriatic Sea (Italy): geometry and characteristics of deep-water channels and sediment waves, Marine and Petroleum," *Geology*, vol. 42, pp. 30–49, 2013.

[85] L. Vezzani and F. Ghisetti, "Carta geologica dell'Abruzzo, 2 sheets, scale 1:100.000," S.E.L.C.A., Firenze, 1998.

[86] ISPRA, Istituto Superiore per la Protezione e la Ricerca Ambientale, "Geological map of Italy at scale 1:100,000, sheets 140, 141, 146-148, 152-155, 160-163, 173, 174," 2021, http://sgi.isprambiente.it/geologia100k/centro.aspx.

[87] ISPRA, Istituto Superiore per la Protezione e la Ricerca Ambientale, "Geological map of Italy at scale 1:50.000, sheet 361 'Chieti'," 2010, http://www.isprambiente.gov.it/Media/carg/361_CHIETI/Foglio.html.

[88] ISPRA, Istituto Superiore per la Protezione e la Ricerca Ambientale, "Geological map of Italy at scale 1:50.000, sheet 351 'Pescara'," 2010,http://www.isprambiente.gov.it/Media/carg/351_PESCARA/Foglio.html.

[89] G. Lavecchia, F. Ferrarini, F. Brozzetti, R. de Nardis, P. Boncio, and L. Chiaraluce, "From surface geology to aftershock analysis: constraints on the geometry of the L'Aquila 2009 seismogenic fault system," *Italian Journal of Geosciences*, vol. 131, pp. 330–347, 2012.

[90] F. Ferrarini, G. Lavecchia, R. de Nardis, and F. Brozzetti, "Fault geometry and active stress from earthquakes and field geology data analysis: the Colfiorito 1997 and L'Aquila 2009 cases (central Italy)," *Pure and Applied Geophysics*, vol. 172, no. 5, pp. 1079–1103, 2015.

[91] F. Ferrarini, P. Boncio, R. de Nardis et al., "Segmentation pattern and structural complexities in seismogenic extensional settings: the North Matese fault system (Central Italy)," *Journal of Structural Geology*, vol. 95, pp. 93–112, 2017.

[92] G. Lavecchia, G. M. Adinolfi, R. de Nardis et al., "Multidisciplinary inferences on a newly recognized active east-dipping extensional system in Central Italy," *Terra Nova*, vol. 29, no. 1, pp. 77–89, 2017.

[93] F. Brozzetti, P. Boncio, D. Cirillo et al., "High-resolution field mapping and analysis of the August–October 2016 coseismic surface faulting (central Italy earthquakes): slip distribution, parameterization, and comparison with global earthquakes," *Tectonics*, vol. 38, no. 2, pp. 417–439, 2019.

[94] D. Scrocca, E. Carminati, C. Doglioni, and D. Marcantoni, "Slab retreat and active shortening along the central-northern Apennines," in *Thrust Belts and Foreland Basins*, pp. 471–487, Springer, Berlin, Heidelberg, 2007.

[95] ISPRA, Servizio Geologico d'Italia, *Note Illustrative della Carta Geologica d'Italia alla scala 1:50,000*, Foglio 339 Teramo, 2010, http://www.isprambiente.gov.it/Media/carg/339_TERAMO/Foglio.html.

[96] L. Vezzani, F. Ghisetti, and A. Festa, *Carta Geologica del Molise, 1 sheet, scale 1:100,000*, S.E.L.CA, Firenze, 2004.

[97] A. W. Bally, L. Burbi, C. Cooper, and R. Ghelardoni, "Balanced sections and seismic reflection profiles across the

central Apennines," *Memorie della Societa Geologica Italiana*, vol. 35, pp. 257–310, 1986.

[98] G. Lavecchia, "The Tyrrhenian-Apennines system: structural setting and seismotectogenesis," *Tectonophysics*, vol. 147, pp. 263–296, 1988.

[99] M. Mattei, R. Funiciello, and C. Kissel, "Paleomagnetic and structural evidence of Neogene block rotation in the Central Apennines, Italy," *Journal Geophysical Research*, vol. 100, pp. 17863–17883, 1995.

[100] F. Speranza, L. Sagnotti, and M. Mattei, "Tectonics of the Umbria-Marche-Romagna Arc (central-northern Apennines, Italy): new paleomagnetic approach," *Journal Geophysical Research*, vol. 102, pp. 3153–3166, 1997.

[101] S. Satolli and F. Calamita, "Differences and similarities between the central and the southern Apennines (Italy): examining the Gran Sasso versus the Matese-Frosolone salients using paleomagnetic, geological, and structural data," *Journal Geophysical Research*, vol. 113, p. B10101, 2008.

[102] A. Cinque, E. Patacca, P. Scandone, and M. Tozzi, "Quaternary kinematic evolution of the Southern Apennines. Relationship between surface geological features and lithospheric structures," *Annali di Geofisica*, vol. 36, pp. 249–260, 1993.

[103] E. Centamore and S. Nisio, "Effects of uplift and tilting in the central-northern Apennines, Italy," *Quaternary International*, vol. 101–102, pp. 93–101, 2003.

[104] V. Bracone, A. Amorosi, P. P. C. Aucelli et al., "The Pleistocene tectono-sedimentary evolution of the Apenninic foreland basin between Trigno and Fortore rivers (Southern Italy) through a sequence stratigraphic perspective," *Basin Research*, vol. 24, no. 2, pp. 1–21, 2011.

[105] P. P. C. Aucelli, "Indizi geomorfologici di tettonica plioquaternaria sul piedimonte adriatico dell'Appennino abruzzese," *Il Quaternario*, vol. 9, pp. 299–302, 1996.

[106] P. P. C. Aucelli, A. Cinque, and G. Robustelli, "Evoluzione quaternaria del tratto di Avanfossa Appenninica compresa tra Larino (Campobasso) e Apricena (Foggia)," *Dati preliminari: Il Quaternario*, vol. 10, pp. 453–460, 1997.

[107] L. D'Alessandro, E. Miccadei, and T. Piacentini, "Morphotectonic study of the lower Sangro River valley (Abruzzi, Central Italy)," *Geomorphology*, vol. 102, no. 1, pp. 145–158, 2008.

[108] M. Della Seta, M. del Monte, P. Fredi et al., "Morphotectonic evolution of the Adriatic piedmont of the Apennines: an advancement in the knowledge of the Marche-Abruzzo border area," *Geomorphology*, vol. 102, no. 1, pp. 119–129, 2008.

[109] A. Malinverno and W. B. F. Ryan, "Extension in the Tyrrhenian sea and shortening in the Apennines as result of arc migration driven by sinking of the lithosphere," *Tectonics*, vol. 5, no. 2, pp. 227–245, 1986.

[110] E. Patacca, R. Sartori, and P. Scandone, "Tyrrhenian basin and Apennine arc. Kinematic relations since Late Tortonian times," *Memorie della Societa' Geologica Italiana*, vol. 45, pp. 425–451, 1990.

[111] F. Galadini and P. Galli, "Active tectonics in the Central Apennines (Italy)-input data for seismic hazard assessment," *Natural Hazards*, vol. 22, no. 3, pp. 225–268, 2000.

[112] C. Bosi, F. Galadini, B. Giaccio, P. Messina, and A. Sposato, "Plio-Quaternary continental deposits in the Latium-Abruzzi Apennines: the correlation of geological events across different intermontane basins," *Il Quaternario Italian Journal of Quaternary Sciences*, vol. 16, pp. 55–76, 2003.

[113] P. Boncio, G. Lavecchia, and B. Pace, "Defining a model of 3D seismogenic sources for seismic hazard assessment applications: the case of central Apennines (Italy)," *Journal of Seismology*, vol. 8, no. 3, pp. 407–425, 2004.

[114] P. Boncio and G. Lavecchia, "A structural model for active extension in Central Italy," *Journal of Geodynamics*, vol. 29, no. 3-5, pp. 233–244, 2000.

[115] P. Galli, B. Giaccio, P. Messina et al., "Middle to Late Pleistocene activity of the northern Matese fault system (southern Apennines, Italy)," *Tectonophysics*, vol. 699, pp. 61–81, 2017.

[116] P. Bordoni and G. Valensise, "Deformation of the 125ka marine terrace in Italy: tectonic implications," in *Coastal Tectonics: Geological Society of London*, I. Stewart and C. Vita-Finzi, Eds., vol. 146 of Special Publication, pp. 71–110, 1998.

[117] R. Westaway, "Quaternary uplift of southern Italy," *Journal of Geophysical Research*, vol. 98, no. B12, pp. 21741–21772, 1993.

[118] C. Doglioni, M. Tropeano, F. Mongelli, and P. Pieri, "Middle-Late Pleistocene uplift of Puglia: an "anomaly" in the Apenninic foreland," *Memorie della Societa Geologica Italiana*, vol. 51, pp. 101–117, 1996.

[119] F. Calamita, M. Coltorti, P. Pieruccini, and A. Pizzi, "Evoluzione strutturale e morfogenesi plio-quaternaria dell'appennino umbro-marchigiano tra il preappennino umbro e la costa adriatica," *Bollettino della Società Geologica Italiana*, vol. 118, pp. 125–139, 1999.

[120] N. D'Agostino, C. Faccenna, S. Corrado, and R. Funiciello, "Geological constraints on the evolution of the Adriatic subduction and uplift of the Apennines (Italy)," *Geophysical Research Abstracts*, vol. 1, no. 63, 1999.

[121] C. Bartolini, N. D'Agostino, and F. Dramis, "Topography, exhumation and drainage network evolution of the Apennines," *Episodes*, vol. 26, no. 3, pp. 212–216, 2003.

[122] C. Doglioni, "A proposal for the kinematic modelling of W-dipping subductions - possible applications to the Tyrrhenian-Apennines system," *Terra Nova*, vol. 3, no. 4, pp. 423–434, 1991.

[123] S. Kruse and L. H. Royden, "Bending and unbending of an elastic lithosphere: the Cenozoic history of the Apennine and Dinaride foredeep basins," *Tectonics*, vol. 13, no. 2, pp. 278–302, 1994.

[124] G. Bertotti, V. Picotti, C. Chilovi, R. Fantoni, S. Merlini, and A. Mosconi, "Neogene to Quaternary sedimentary basins in the south Adriatic (Central Mediterranean): foredeeps and lithospheric buckling," *Tectonics*, vol. 20, no. 5, pp. 771–787, 2001.

[125] G. P. Cavinato and P. G. D. Celles, "Extensional basins in the tectonically bimodal central Apennines fold-thrust belt, Italy: response to corner flow above a subducting slab in retrograde motion," *Geology*, vol. 27, no. 10, pp. 955–958, 1999.

[126] Z. Gvirtzman and A. Nur, "Residual topography, lithospheric structure and sunken slabs in the central Mediterranean," *Earth and Planetary Science Letters*, vol. 187, no. 1-2, pp. 117–130, 2001.

[127] C. Faccenna, T. W. Becker, M. S. Miller, E. Serpelloni, and S. D. Willett, "Isostasy, dynamic topography, and the elevation of the Apennines of Italy," *Earth and Planetary Science Letters*, vol. 407, pp. 163–174, 2014.

[128] P. P. C. Aucelli, A. Cinque, and C. Rosskopf, "Geomorphological map of the Trigno basin (Italy): explanatory notes,"

Geografia Fisica e Dinamica Quaternaria, vol. 24, pp. 3–12, 2001.

[129] P. Aucelli, V. Amato, M. Cesarano et al., "New morphostratigraphic and chronological constraints for the Quaternary paleosurfaces of the Molise Apennine (southern Italy)," *Geologica Carpathica*, vol. 62, no. 1, pp. 17–26, 2011.

[130] T. Urbano, T. Piacentini, and M. Buccolini, "Morphotectonics of the Pescara River basin (Central Italy)," *Journal of Maps*, vol. 13, no. 2, pp. 511–520, 2017.

[131] W. Schwanghart and N. J. Kuhn, "TopoToolbox: a set of Matlab functions for topographic analysis," *Environmental Modelling & Software*, vol. 25, no. 6, pp. 770–781, 2010.

[132] W. Schwanghart and D. Scherler, "Short Communication: TopoToolbox 2 – MATLAB-based software for topographic analysis and modeling in Earth surface sciences," *Earth Surface Dynamics*, vol. 2, no. 1, pp. 1–7, 2014.

[133] A. M. Forte and K. X. Whipple, "Short communication: The topographic analysis kit (TAK) for TopoToolbox," *Earth Surf. Dynam*, vol. 7, no. 1, pp. 87–95, 2019.

[134] ViDEPI Project, *Visibility of Petroleum Exploration Data in Italy*, Ministry for Economic Development DGRME - Italian Geological Society - Assomineraria, 2021, https://www.videpi.com/videpi/videpi.asp#.

[135] R. Bürgmann, R. Arrowsmith, T. Dumitru, and R. McLaughlin, "Rise and fall of the southern Santa Cruz Mountains, California, from fission tracks, geomorphology, and geodesy," *Journal of Geophysical Research*, vol. 99, no. B10, pp. 20181–20202, 1994.

[136] T. F. Bullard and W. R. Lettis, "Quaternary fold deformation associated with blind thrust faulting, Los Angeles Basin, California," *Journal of geophysical research Planets*, vol. 98, no. B5, pp. 8349–8369, 1993.

[137] J. T. Hack, *Studies of longitudinal stream profiles*, U.S. Geological Survey, Professional Paper 294-B, Virginia and Maryland, 1957.

[138] J. J. Flint, "Stream gradient as a function of order, magnitude, and discharge," *Water Resources Research*, vol. 10, no. 5, pp. 969–973, 1974.

[139] N. Snyder, K. X. Whipple, G. E. Tucker, and D. J. Merritts, "Landscape response to tectonic forcing: digital elevation model analysis of stream profiles in the Mendocino triple junction region, northern California," *Geological Society of America Bulletin*, vol. 112, no. 8, pp. 1250–1263, 2000.

[140] D. R. Montgomery and E. Foufoula-Georgiou, "Channel network source representation using digital elevation models," *Water Resources Research*, vol. 29, no. 12, pp. 3925–3934, 1993.

[141] J. Stock and W. E. Dietrich, "Valley incision by debris flows: evidence of a topographic signature," *Water Resources Research*, vol. 39, no. 4, p. 1089, 2003.

[142] A. D. Howard, "A detachment-limited model of drainage basin evolution," *Water Resources Research*, vol. 30, no. 7, pp. 2261–2285, 1994.

[143] L. Sklar and W. E. Dietrich, "River longitudinal profiles and bedrock incision models: stream power and the influence of sediment supply," in *Rivers over Rock: Fluvial Processes in Bedrock Channels*, K. J. Tinkler and E. E. Wohl, Eds., pp. 237–260, AGU Press, Washington, D.C., 1998.

[144] J. T. Perron and L. Royden, "An integral approach to bedrock river profile analysis," *Earth Surface Processes and Landforms*, vol. 38, no. 6, pp. 570–576, 2013.

[145] A. Duvall, E. Kirby, and D. Burbank, "Tectonic and lithologic controls on bedrock channel profiles and processes in coastal California," *Journal of Geophysical Research*, vol. 109, no. F3, article F03002, 2004.

[146] U. Crescenti, M. L. Milia, and G. Rusciadelli, "Stratigraphic and structural evolution of the Pliocene Abruzzi basin (Central Apennines, Italy)," *Bollettino della Società Geologica Italiana*, vol. 123, pp. 163–173, 2004.

[147] M. R. Barchi, A. De Feyter, M. B. Magnani, G. Minelli, G. Pialli, and M. Sotera, "The structural style of the Umbria-Marche fold and thrust belt," *Memorie della Societa Geologica Italiana*, vol. 52, pp. 557–578, 1998.

[148] M. A. Foster and H. M. Kelsey, "Knickpoint and knickzone formation and propagation: South Fork Eel River, northern California," *Geosphere*, vol. 8, no. 2, pp. 403–416, 2012.

[149] V. Scisciani and R. Montefalcone, "Evoluzione neogenico-quaternaria del fronte della catena centro-appenninica: vincoli dal bilanciamento sequenziale di una sezione geologica regionale," *Bollettino della Società Geologica Italiana*, vol. 124, pp. 579–599, 2005.

[150] F. Antonioli, E. Bard, E. K. Potter, S. Silenzi, and S. Improta, "215-ka history of sea-level oscillations from marine and continental layers in Argentarola Cave speleothems (Italy)," *Global and Planetary Change*, vol. 43, no. 1-2, pp. 57–78, 2004.

[151] A. M. Forte, B. J. Yanites, and K. X. Whipple, "Complexities of landscape evolution during incision through layered stratigraphy with contrasts in rock strength," *Earth Surf. Process Landforms*, vol. 41, no. 12, pp. 1736–1757, 2016.

[152] B. J. Yanites, J. K. Becker, H. Madritsch, M. Schnellmann, and T. A. Ehlers, "Lithologic effects on landscape response to base level changes: a modeling study in the context of the eastern Jura Mountains, Switzerland," *Journal of Geophysical Research: Earth Surface*, vol. 122, no. 11, pp. 2196–2222, 2017.

[153] J. D. Jansen, A. T. Codilean, P. Bishop, and T. B. Hoey, "Scale dependence of lithological control on topography: bedrock channel geometry and catchment morphometry in western Scotland," *The Journal of Geology*, vol. 118, no. 3, pp. 223–246, 2010.

[154] A. F. García, Z. Zhu, T. L. Ku, O. A. Chadwick, and J. Chacón Montero, "An incision wave in the geologic record, Alpujarran Corridor, southern Spain (Almería)," *Geomorphology*, vol. 60, no. 1-2, pp. 37–72, 2004.

[155] J. R. Miller, "The influence of bedrock geology on knickpoint development and channel-bed degradation along downcutting streams in south-Central Indiana," *Journal of Geology*, vol. 99, no. 4, pp. 591–605, 1991.

[156] Z. Alexandrowicz, "Geologically controlled waterfall types in the Outer Carpathians," *Geomorphology*, vol. 9, no. 2, pp. 155–165, 1994.

[157] S. J. Boulton, M. Stokes, and A. E. Mather, "Transient fluvial incision as an indicator of active faulting and Plio- Quaternary uplift of the Moroccan High Atlas," *Tectonophysics*, vol. 633, pp. 16–33, 2014.

[158] A. Replumaz, M. San José, A. Margirier et al., "Tectonic control on rapid Late Miocene — Quaternary incision of the Mekong River knickzone, Southeast Tibetan Plateau," *Tectonics*, vol. 39, no. 2, 2020.

[159] F. Riguzzi, A. Tertulliani, and C. Gasparini, "Study of the seismic sequence of Porto San Giorgio (Marche), 3 July 1987," *Il Nuovo Cimento*, vol. 12, no. 4, pp. 453–466, 1989.

[160] C. Gasparini, A. Maramai, and M. Vecchi, "Il terremoto del Montefeltro del 5 luglio 1987," in *Proceedings of the 8th G.N.G.T.S.*, pp. 493–501, Rome, 1989.

[161] S. Pondrelli, S. Salimbeni, G. Ekström, A. Morelli, P. Gasperini, and G. Vannucci, "The Italian CMT dataset from 1977 to the present," *Physics of the Earth and Planetary Interiors*, vol. 159, no. 3-4, pp. 286–303, 2006.

[162] G. Vannucci and P. Gasperini, "The new release of the database of Earthquake Mechanisms of the Mediterranean Area (EMMA version 2)," *Annals of Geophysics*, vol. 47, 1 Supplement, pp. 307–334, 2009.

[163] A. Frepoli and A. Amato, "Contemporaneous extension and compression in the Northern Apennines from earthquake faultplane solutions," *Geophys J Int*, vol. 129, no. 2, pp. 368–388, 1997.

[164] G. de Luca, M. Cattaneo, G. Monachesi, and A. Amato, "Seismicity in Central and Northern Apennines integrating the Italian national and regional networks," *Tectonophysics*, vol. 476, no. 1-2, pp. 121–135, 2009.

[165] L. Scognamiglio, E. Tinti, and M. Quintiliani, *Time domain moment tensor [data set]*, Istituto Nazionale di Geofisica e Vulcanologia (INGV), 200610.13127/TDMT.

[166] A. Frepoli, G. B. Cimini, P. de Gori et al., "Seismic sequences and swarms in the Latium-Abruzzo-Molise Apennines (central Italy): new observations and analysis from a dense monitoring of the recent activity," *Tectonophysics*, vol. 712-713, pp. 312–329, 2017.

[167] M. A. Romano, R. de Nardis, M. Garbin et al., "Temporary seismic monitoring of the Sulmona area (Abruzzo, Italy): a quality study of microearthquake locations," *Natural Hazards and Earth System Sciences*, vol. 13, no. 11, pp. 2727–2744, 2013.

[168] G. Lavecchia, R. de Nardis, F. Ferrarini, D. Cirillo, S. Bello, and F. Brozzetti, "Regional seismotectonic zonation of hydrocarbon fields in active thrust belts: a case study from Italy," in *Building Knowledge for Geohazard Assessment and Management in the Caucasus and Other Orogenic Regions*, NATO Science for Peace and Security Series C: Environmental Security, F. L. Bonali, F. Pasquaré Mariotto, and N. Tsereteli, Eds., Springer, Dordrecht, 2021.

[169] P. Petricca, E. Carminati, and C. Doglioni, "The decollement depth of active thrust faults in Italy: implications on potential earthquake magnitude," *Tectonics*, vol. 38, no. 11, pp. 3990–4009, 2019.

[170] S. Bagh, L. Chiaraluce, P. de Gori et al., "Background seismicity in the Central Apennines of Italy: the Abruzzo region case study," *Tectonophysics*, vol. 444, no. 1-4, pp. 80–92, 2007.

[171] R. de Nardis, M. Garbin, G. Lavecchia et al., "A temporary seismic monitoring of the Sulmona area (Abruzzo, Italy) for seismotectonic purposes," *Bollettino di Geofisica Teorica ed Applicata*, vol. 52, pp. 651–666, 2011.

[172] C. Chiarabba, P. de Gori, and F. M. Mele, "Recent seismicity of Italy: Active tectonics of the central Mediterranean region and seismicity rate changes after the Mw 6.3 L'Aquila earthquake," *Tectonophysics*, vol. 638, pp. 82–93, 2015.

[173] G. Bertotti, Casolari, and Picotti, "The Gargano promontory: a Neogene contractional belt within the Adriatic plate," *Terra Nova*, vol. 11, no. 4, pp. 168–173, 1999.

[174] E. Tondi, L. Piccardi, S. Cacon, B. Kontny, and G. Cello, "Structural and time constraints for dextral shear along the seismogenic Mattinata Fault (Gargano, southern Italy)," *Journal of Geodynamics*, vol. 40, no. 2-3, pp. 134–152, 2005.

[175] D. di Bucci and S. Mazzoli, "The October–November 2002 Molise seismic sequence (southern Italy): an expression of Adria intraplate deformation," *Journal of the Geological Society*, vol. 160, no. 4, pp. 503–506, 2003.

[176] G. Valensise, D. Pantosti, and R. Basili, "Seismology and tectonic setting of the 2002 Molise, Italy, Earthquake," *Earthquake Spectra*, vol. 20, 1_Supplement, pp. 23–37, 2004.

[177] G. M. Adinolfi, R. de Matteis, A. Orefice et al., "The September 27, 2012, ML 4.1, Benevento earthquake: a case of strike-slip faulting in Southern Apennines (Italy)," *Tectonophysics*, vol. 660, pp. 35–46, 2015.

[178] J. R. Arrowsmith and M. R. Strecker, "Seismotectonic range-front segmentation and mountain belt growth in the Pamir-Alai region, Kyrgyzstan (India-Eurasia collision zone)," *GSA Bulletin*, vol. 111, no. 11, pp. 1665–1683, 1999.

[179] K. M. Cohen and P. L. Gibbard, "Global chronostratigraphical correlation table for the last 2.7 million years, version 2019 QI-500," *Quaternary International*, vol. 500, pp. 20–31, 2019.

[180] K. M. Cohen, S. C. Finney, P. L. Gibbard, and J. X. Fan, "The ICS International Chronostratigraphic Chart," *Episodes*, vol. 36, no. 3, pp. 199–204, 2013.

[181] E. Miccadei, C. Carabella, G. Paglia, and T. Piacentini, "Paleo-drainage network, morphotectonics, and fluvial terraces: clues from the Verde Stream in the Middle Sangro River (Central Italy)," *Geosciences*, vol. 8, no. 9, p. 337, 2018.

[182] E. Miccadei, T. Piacentini, F. Gerbasi, and F. Daverio, "Morphotectonic map of the Osento River basin (Abruzzo, Italy), scale 1:30,000," *Journal of Maps*, vol. 8, no. 1, pp. 62–73, 2012.

[183] ISPRA, Istituto Superiore per la Protezione e la Ricerca Ambientale, *Geological Map of Italy at Scale 1:50,000*, sheet 372 Vasto, 2010, https://www.isprambiente.gov.it/Media/carg/372_VASTO/Foglio.html.